iScience

CellPress

Article

Cross Talk between eIF2α and eEF2 Phosphorylation Pathways Optimizes Translational Arrest in Response to Oxidative Stress

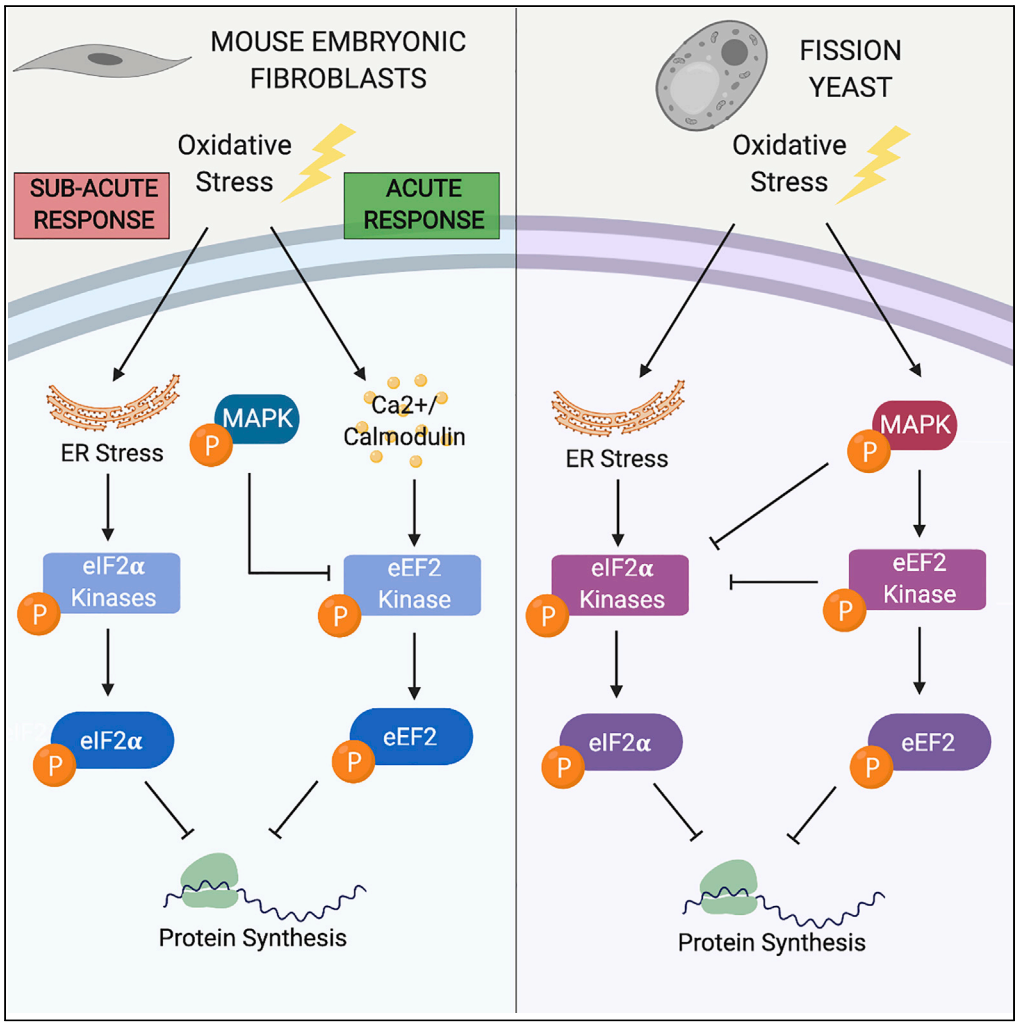

Marisa Sanchez, Yingying Lin, Chih-Cheng Yang, Philip McQuary, Alexandre Rosa Campos, Pedro Aza Blanc, Dieter A. Wolf

marisa3593@gmail.com (M.S.)
dwolf@xmu.edu.cn (D.A.W.)

HIGHLIGHTS

Oxidative stress-induced translation arrest is independent of eIF2α phosphorylation

Oxidative stress blocks translation elongation

Oxidative stress triggers eEF2 kinase activation

eEF2K KO cells are hypersensitive to oxidative stress

Sanchez et al., iScience *20*, 466–480
October 25, 2019
https://doi.org/10.1016/j.isci.2019.09.031

iScience

CellPress

Article

Cross Talk between eIF2α and eEF2 Phosphorylation Pathways Optimizes Translational Arrest in Response to Oxidative Stress

Marisa Sanchez,[1,3,*] Yingying Lin,[2] Chih-Cheng Yang,[1] Philip McQuary,[1] Alexandre Rosa Campos,[1] Pedro Aza Blanc,[1] and Dieter A. Wolf[1,2,*]

SUMMARY

The cellular stress response triggers a cascade of events leading to transcriptional reprogramming and a transient inhibition of global protein synthesis, which is thought to be mediated by phosphorylation of eukaryotic initiation factor-2α (eIF2α). Using mouse embryonic fibroblasts (MEFs) and the fission yeast *S. pombe*, we report that rapid translational arrest and cell survival in response to hydrogen peroxide-induced oxidative stress do not rely on eIF2α kinases and eIF2α phosphorylation. Rather, H_2O_2 induces a block in elongation through phosphorylation of eukaryotic elongation factor 2 (eEF2). Kinetic and dose-response analyses uncovered cross talk between the eIF2α and eEF2 phosphorylation pathways, indicating that, in MEFs, eEF2 phosphorylation initiates the acute shutdown in translation, which is maintained by eIF2α phosphorylation. Our results challenge the common conception that eIF2α phosphorylation is the primary trigger of translational arrest in response to oxidative stress and point to integrated control that may facilitate the survival of cancer cells.

INTRODUCTION

mRNA translation, the energetically most demanding step in gene expression, is tightly regulated (Buttgereit and Brand, 1995; Rolfe and Brown, 1997; Sonenberg and Hinnebusch, 2009). Although translation is conceptually separated into discrete biochemical steps—initiation, elongation, termination, and ribosome recycling (Hershey et al., 2012)—regulation may occur in a more integrated fashion *in vivo*, affecting multiple steps simultaneously (Richter and Coller, 2015; Sha et al., 2009).

One of the best-studied regulatory pathways centers on eukaryotic initiation factor 2 (eIF2), a GTP-binding protein containing three subunits, α, β, and γ. As part of the ternary complex (also comprising of the initiator tRNA-methionine and GTP), eIF2 joins the 40S ribosome in scanning the mRNA for an initiation codon. After the 60S ribosomal subunit is added upon start codon recognition, GTP is hydrolyzed, leading to the release of eIF2-GDP. To be reused in subsequent rounds of initiation, eIF2 bound to GDP must be converted to eIF2-GTP by the guanine nucleotide exchange factor eIF2B. Phosphorylation of eukaryotic initiation factor-2α (eIF2α) on residue S51 increases its affinity for eIF2B but reduces its GDP to GTP exchange activity thus resulting in reduced levels of functional eIF2 leading to inhibition of global mRNA translation (Pavitt, 2018).

eIF2α phosphorylation is pivotal for ablating translation in response to environmental stress (Wek et al., 2006). Eukaryotic cells recognize and process diverse stress signals to elicit programs of gene expression that are designed to alleviate cellular damage, or alternatively induce apoptosis. Important contributors to this stress response are a family of four protein kinases (PERK, PKR, GCN2, and HRI) that phosphorylate eIF2α on Ser51 and inhibit protein synthesis, thereby conserving energy and facilitating the reprogramming of gene expression and signaling to restore protein homeostasis (Wek, 2018; Wek et al., 2006). However, previous reports in yeast showed that the eIF2α kinase Gcn2 and the eIF2α phosphorylation site are dispensable for translational inhibition in response to H_2O_2 and UV light (Knutsen et al., 2015; Shenton et al., 2006). These studies also provided evidence that H_2O_2 impedes translation elongation, although the underlying signaling and the interplay between effects on initiation and elongation remained unclear. Likewise, it remained open whether control at the level of elongation is conserved in mammalian cells.

Even though initiation of translation is considered the most important regulatory step, there is increasing attention on mechanisms that affect other steps, in particular elongation (Richter and Coller, 2015). Two

[1]Sanford Burnham Prebys Medical Discovery Institute, La Jolla, CA 92037, USA

[2]School of Pharmaceutical Sciences, Fujian Provincial Key Laboratory of Innovative Drug Target Research and Center for Stress Signaling Networks, Xiamen University, Xiamen 361102, China

[3]Lead Contact

*Correspondence: marisa3593@gmail.com (M.S.), dwolf@xmu.edu.cn (D.A.W.)

https://doi.org/10.1016/j.isci.2019.09.031

important elongation regulatory factors are eukaryotic elongation factor 2 (eEF2) and its kinase, eEF2K. Eukaryotic elongation factor 2 kinase (eEF2K) is a Ca^{2+}/calmodulin (CaM)-dependent kinase, which negatively modulates protein synthesis by phosphorylating eEF2 (Kenney et al., 2014; Tavares et al., 2014). Phosphorylation at Thr56 within the GTP-binding domain of eEF2 prevents its recruitment to ribosomes and thus blocks elongation (Carlberg et al., 1990). eEF2K is subject to regulation by cellular nutrient and energy status. Nutrient depletion is associated with activation of eEF2K via AMPK and inhibition of TORC1 signaling pathways, resulting in increased autophagy and cell survival (Kruiswijk et al., 2012). The frequent overexpression of eEF2K in human cancers may thus confer tumor cell adaptation to microenvironmental nutrient stress (Fu et al., 2014). As inhibition of eEF2K's survival function augments ER stress-induced apoptosis, eEF2K may be an anti-cancer drug target (Cheng et al., 2013; Fu et al., 2014).

The tumorigenic state is marked by alterations activating a mutually reinforcing network of metabolic, genotoxic, proteotoxic, and oxidative stresses (Gorrini et al., 2013; Luo et al., 2009). Oxidative stress is particularly significant because it can both induce and result from the other forms of stress. Moderate levels of reactive oxygen species (ROS) may contribute to tumorigenesis either as signaling molecules or by inducing DNA mutations (Gorrini et al., 2013). To sustain survival under high ROS levels typically seen in tumors, cells rely on sophisticated stress defense pathways that have been proposed as cancer drug targets (Luo et al., 2009). In particular, overwhelming oxidative stress defense either through inhibition of ROS scavenging or through augmenting ROS levels by chemotherapeutics or inducers of protein misfolding has been proposed as a promising strategy (Gorrini et al., 2013; Trachootham et al., 2009; Wolf, 2014).

The important roles of ROS-mediated oxidative stress in cancer promotion and therapy contrast with the limited understanding of the effects of ROS on global gene expression programs that direct cell adaptation or death decisions. Although effects on transcription, mediated through prominent transcription factors such as nuclear factor (NF)-κB, AP1, and NRF2, are well documented (Trachootham et al., 2008), post-transcriptional levels of control remain largely unassessed. The prevailing dogma that stress impacts gene expression post-transcriptionally through shutdown of global translation as a consequence of eIF2α phosphorylation (Wek, 2018; Wek et al., 2006) has been qualified by studies in yeast (Knutsen et al., 2015; Shenton et al., 2006). To gain further insight into post-transcriptional control of gene expression in response to oxidative stress, we have addressed mechanisms conserved in mammalian cells and in fission yeast. Our data suggest that an integrated response at the levels of translation initiation and elongation coordinates survival under oxidative stress.

RESULTS

Oxidative Stress-Induced Transcriptome Changes Differ Depending on the Status of eIF2α Phosphorylation

To gain insight into layers of gene expression in response to oxidative stress, we obtained transcriptomic profiles by RNA sequencing. Immortalized mouse embryonic fibroblasts (MEFs) were used that carried either wild-type eIF2α (WT) or a point mutant in which the inhibitory Ser 51 phosphorylation site was replaced by alanine (eIF2α^{S51A}) thus rendering eIF2α insensitive to kinase-mediated inhibition and translational shutdown in response to stress (Back et al., 2009; McEwen et al., 2005). To monitor acute and prolonged responses to oxidative stress, cells were exposed for either 15 or 120 min to 500 μM H_2O_2 and triplicate RNA samples were obtained for sequencing. Although eIF2α^{S51A} MEFs had ~2-fold higher levels of cellular ROS at baseline, treatment with 500 μM H_2O_2 led to a robust and comparable increase in ROS levels in both cell lines (Figures S1A and S1B).

Significant H_2O_2-induced changes in mRNA levels ($p \leq 0.05$) at both treatment time points were identified with 613 mRNAs changing in wild-type MEFs and 982 in eIF2α^{S51A} mutant MEFs. There was partial overlap in the responsive mRNAs, but an approximately equal number of changes were unique to each cell line (Figure S1C). In WT cells, the transcriptional response peaked at 15 min (Figure 1A) and mostly consisted of downregulated mRNAs that encoded factors involved in protein synthesis (Figure 1B). Many of these changes were already present in eIF2α^{S51A} MEFs at baseline (untreated, 0 min and Figures S1D and S1E), indicating that the mutant cells display a partially activated stress response, possibly as a result of higher basal ROS levels (Figures S1A and S1B). Since mRNAs encoding protein synthesis factors, including ribosomal proteins, are typically among the most highly translated in unstressed cells, their acute

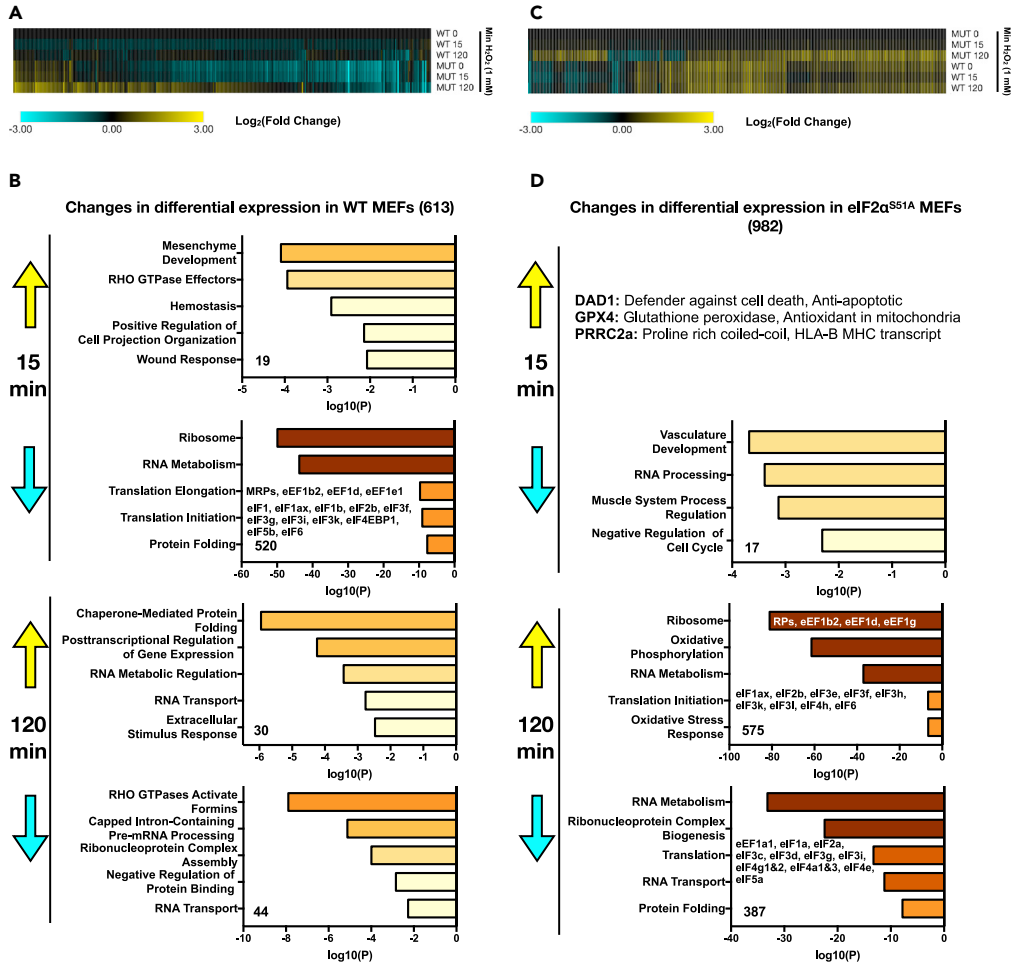

Figure 1. Transcriptome Changes under Oxidative Stress

(A) WT and eIF2α^{S51A} MEFs were either untreated or treated with H_2O_2 (500 μM) for 15 or 120 min. Total RNA was extracted and analyzed by RNA-seq. The data represent a compilation of significant changes in expression ($p \leq 0.05$) found in WT MEFs at either the 15- or 120-min time point. Results are normalized to untreated WT MEFs at time 0 and displayed as a clustered heatmap. Upregulated transcripts are shown in yellow and downregulated transcripts in blue. See Data S1 and S2 for complete list (GEO: GSE137409).

(B) Individual list of H_2O_2-induced and H_2O_2-repressed mRNAs (±3-fold change, $p \leq 0.05$) in WT MEFs were loaded into Metascape, and the pathways enriched are indicated at each time point. Colored boxes represent either upregulated (yellow) or downregulated (blue) pathways. See Data S1 and S2 for a complete list (GEO accession number GSE137409).

(C) WT and eIF2α^{S51A} MEFs were either untreated or treated with H_2O_2 (500 μM) for 15 or 120 min. Total RNA was extracted and analyzed by RNA-seq. The data represent a compilation of significant changes in expression ($p \leq 0.05$) found in eIF2α^{S51A} MEFs at either the 15- or 120-min time point. Results are normalized to untreated eIF2α^{S51A} MEFs at time 0 and displayed as a clustered heatmap. Upregulated transcripts are shown in yellow and downregulated transcripts in blue. See Data S1 and S2 for a complete list.

(D) Individual list of H_2O_2-induced and H_2O_2-repressed mRNAs (±3-fold change, $p \leq 0.05$) in eIF2α^{S51A} MEFs were loaded into Metascape, and the pathways enriched are indicated at each time point. Colored boxes represent either upregulated (yellow) or downregulated (blue) pathways. See Data S1 and S2 for a complete list.

downregulation may serve to liberate ribosome capacity for the translation of newly induced mRNAs (Lackner et al., 2012; Lee et al., 2011). After 120 min, WT cells induced mRNAs encoding factors involved in protein folding, signifying the recovery phase (Figure 1B).

In contrast, few changes were observed in eIF2α^{S51A} mutant MEFs after 15 min and the response was considerably stronger after 120 min (Figure 1C), indicating that eIF2α^{S51A} mutant MEFs show an overall delayed response to H_2O_2. Unlike WT cells, which displayed mostly a gene repressive pattern, eIF2α^{S51A}

mutant MEFs showed a higher number of mRNAs upregulated than downregulated. Curiously, the pattern in eIF2α^{S51A} MEFs at 120 min was an approximate mirror image of the pattern observed with WT cells at 15 min. The latter downregulated protein synthesis factors, whereas they were upregulated in eIF2α^{S51A} MEFs (Figure 1D). Conversely, protein folding was up in WT cells but down in eIF2α^{S51A} MEFs. In summary, the mRNA profiles indicate that eIF2α phosphorylation substantially shapes gene expression in stressed and unstressed cells. The observed differences in the regulation of mRNAs encoding translation and protein folding factors may reflect distinct translational responses possibly resulting in differential sensitivity to H_2O_2.

Oxidative Stress-Induced Translational Inhibition Is Independent of eIF2α Phosphorylation

To test the above-mentioned idea, WT and eIF2α^{S51A} mutant MEFs were exposed to inducers of oxidative and ER stress, followed by determination of cell viability. Although there was differential sensitivity to the ER stress inducer thapsigargin with eIF2α^{S51A} mutant cells being more sensitive than WT MEFs as described previously (Hiramatsu et al., 2014), both MEF lines showed equal sensitivity to cytotoxicity exerted by hydrogen peroxide (H_2O_2) (Figures 2A and 2B). Likewise, equal sensitivity of both MEF lines was observed for the oxidant tert-butyl hydroperoxide (TBHP).

The same differential response was observed at the level of global protein synthesis. Wild-type MEFs downregulated incorporation of fluorescently labeled amino acids into cellular proteins in response to ER stress inducers tunicamycin (Tm), thapsigargin (Tg), and dithiothreitol (DTT), whereas eIF2α^{S51A} mutant MEFs were less responsive (Figure 2C). In contrast, both wild-type and eIF2α^{S51A} mutant MEFs responded with a ~50% inhibition of amino acid incorporation to challenge with 1 mM hydrogen peroxide (Figure 2C). An equal ~50% inhibition was obtained for both cell lines with the ribosomal elongation blocker cycloheximide (Figure 2C).

Likewise, dose responses for inhibition of protein synthesis by hydrogen peroxide did not differ between wild-type and eIF2α^{S51A} mutant MEFs, with both cell lines showing maximal inhibition at a concentration of 3 mM H_2O_2 (Figure 2D). However, time course measurements with brief 5-min pulses of [^{35}S]-methionine revealed markedly different kinetics of recovery of protein synthesis from insult with 1 mM H_2O_2. Although both cell lines exhibited acute inhibition of protein synthesis within 5 min of exposure to hydrogen peroxide, eIF2α^{S51A} mutant MEFs recovered protein synthesis sooner than wild-type MEFs, returning to pretreatment levels within 60 min (Figure 2E). Recovering wild-type MEFs did not reach pretreatment levels within the 120-min time frame of the experiment.

Although these data confirmed the canonical role of eIF2α phosphorylation as a mediator of ER stress-induced translation inhibition, they revealed an unexpected differential response to oxidative stress. eIF2α phosphorylation is dispensable for immediate translational shutdown following H_2O_2, whereas it is required for maintenance of the inhibition, potentially enabling time-demanding repair and recovery processes.

eIF2α Kinases Are Dispensable for Translational Shutdown and Survival under Oxidative Stress

To gain a more mechanistic understanding of eIF2α phosphorylation-independent translation inhibition under oxidative stress, we investigated the role of eIF2α kinases. For this, we turned to the fission yeast *S. pombe* as a model system owing to its facile genetics and faithful recapitulation of the complexity of eIF2α phosphorylation. Like human cells, *S. pombe* encodes several different eIF2α kinases (Hri1p, Hri2p, Gcn2p) that phosphorylate a conserved serine residue (S52). Strains either carrying a S52A mutation of eIF2α or deleted for all three eIF2α kinases were fully viable as described previously (Berlanga et al., 2010; Tvegård et al., 2007). Remarkably, both strains showed similar inhibition of protein synthesis in response to H_2O_2 as observed in wild-type cells despite being completely deficient in eIF2α phosphorylation (Figures 3A and 3B).

Consistent with the data on inhibition of protein synthesis, neither the eIF2α S52A mutant nor the triple eIF2α kinase-deficient strain was sensitive to H_2O_2 exposure as compared with a strain deleted for the stress-responsive MAP kinase, Sty1p (Figures 3C and S3). In summary, these data strongly suggest that the conserved eIF2α phosphorylation site as well as the kinases modifying it are dispensable for both acute translational shutdown in response to oxidative stress and cell survival.

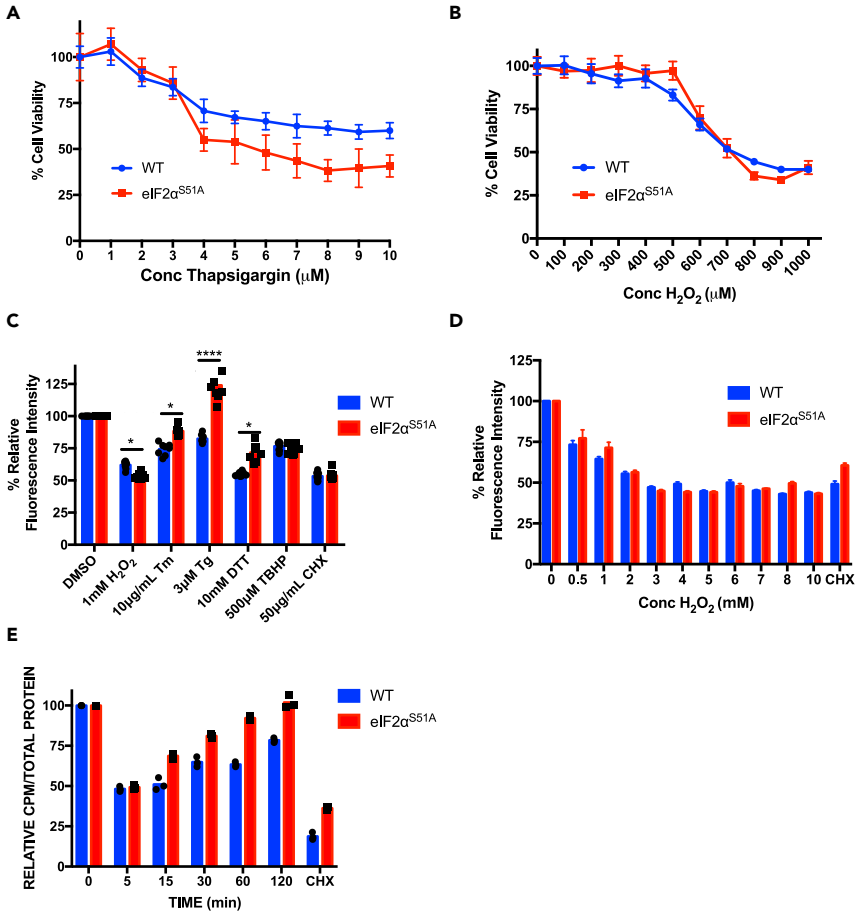

Figure 2. Effect of Hydrogen Peroxide on Viability and Protein Synthesis

(A) Wild-type and eIF2α^{S51A} mutant MEFs were treated with increasing doses (1–10 μM) of the ER stress inducer thapsigargin for 2 h. MTT assay was used to assess cell viability; see Figure S2A for verified results. The graph represents the mean ± standard deviations of 8 replicates.

(B) Wild-type and eIF2α^{S51A} mutant MEFs were treated with the indicated increasing doses (100–1000 μM) of the oxidative stress inducer hydrogen peroxide (H_2O_2) for 2 h. MTT assay was used to assess cell viability, see Figure S2B for verified results. The graph represents the mean ± standard deviations of eight replicates.

(C) Wild-type and eIF2α^{S51A} mutant MEFs were treated with the indicated doses of specific stress inducers: H_2O_2, tunicamycin (Tm), thapsigargin (Tg), dithiothreitol (DTT), and tert-butyl hydroperoxide (TBHP). Cells were treated for 2 h except in the case of tunicamycin, which was added for 4 h. The protein synthesis inhibitor cycloheximide (CHX) was used as a control. Protein synthesis was measured by fluorescently tagging nascent polypeptides and quantifying the fluorescence intensity. The graph represents the normalized mean ± standard deviations of eight replicates. The individual symbols represent individual data points. *p value H_2O_2 = 0.016, p value Tm = 0.017, p value Tg = 8×10^{-6}, p value DTT = 0.013. Statistical significance was determined by t test.

(D) Wild-type and eIF2α^{S51A} mutant MEFs were treated with increasing doses (0.5–10 mM) of H_2O_2 for 1 h. Protein synthesis was measured with a fluorescent tagging assay. CHX, 50 μg/mL, was added for 1 h as a control. The graph represents the normalized mean ± standard deviations of eight replicates.

(E) Wild-type and eIF2α^{S51A} mutant MEFs were treated with 500 μM H_2O_2 for increasing periods (5–120 min). Cells were simultaneously labeled with [^{35}S]-methionine for 5 min. Protein synthesis was measured by quantifying radioactive counts per minute (CPM) and adjusted according to the total amount of protein. The graph represents the normalized mean ± standard deviations of at least two independent experiments each done in triplicates. The individual symbols represent individual data points.

Translation Elongation Is Blocked in the Absence of eIF2α Phosphorylation under Oxidative Stress

To corroborate these findings, we determined the effect of H_2O_2 on the global distribution of ribosomes along a sucrose density gradient. In wild-type cells, H_2O_2 triggered a time-dependent redistribution of

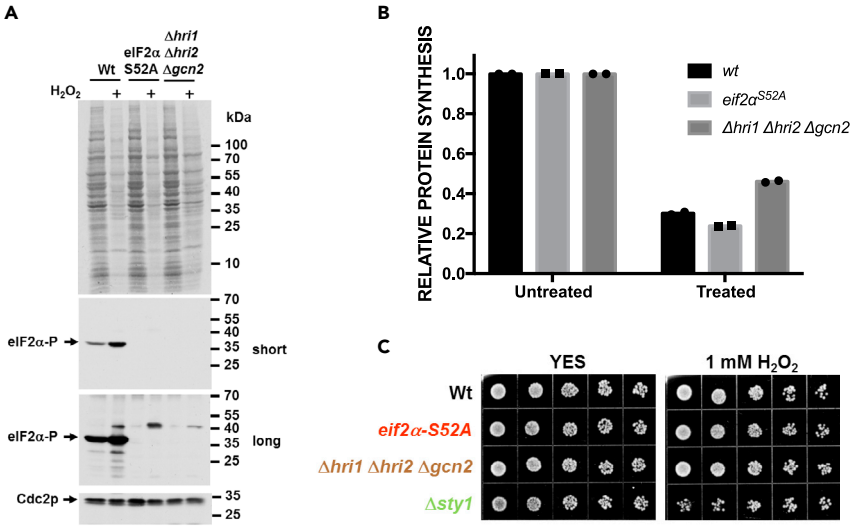

Figure 3. Effect of *S. pombe* eIF2α Phosphorylation Pathway Mutations on Protein Synthesis and Cell Survival

(A) WT, *eIF2α*^{S52A}, and *Δhri1 Δhri2 Δgcn2* strains of *S. pombe* were treated with 1 mM H_2O_2 for 15 min and [^{35}S]-methionine was added for the next 45 min. Total protein was isolated and separated by SDS-PAGE, and protein synthesis was detected by film autoradiography (top panel). The same lysates were analyzed by immunoblotting for eIF2α phosphorylation. Signals for Cdc2p are shown for reference.

(B) The same lysates as described in (A) were TCA precipitated, and [^{35}S]-methionine incorporation was quantified by scintillation counting.

(C) Sensitivity of WT, *eIF2α*^{S52A}, *Δhri1 Δhri2 Δgcn2*, and *Δsty1* strains to H_2O_2 was assessed by spotting 5-fold serial dilutions on plates containing 1 mM H_2O_2.

See Figure S3.

ribosomes from the polysomal to the monosomal 80S fraction, indicating that cells responded to oxidative stress with polysome run-off and suppression of the formation of new polysomes (Figure 4A). Only a marginal polysome to monosome shift was observed in eIF2α^{S51A} mutant MEFs under the same conditions (Figure 4A). This finding suggested that ribosomes do not run off mRNAs in eIF2α^{S51A} mutant MEFs exposed to oxidative stress.

Persistent polyribosome occupancy on mRNA between 5 and 60 min after exposure of eIF2α^{S51A} mutant MEFs to H_2O_2 was in stark contrast to the marked inhibition of amino acid incorporation after only 5 min of H_2O_2 (Figure 2E). This seemingly conflicting data led to the hypothesis that oxidative stress induced a block of translation elongation. Indeed, ribosome transit time (Nielsen and McConkey, 1980) was ~2.5-fold increased in H_2O_2-treated eIF2α^{S51A} mutant MEFs relative to wild-type MEFs, which showed less than a 1.5-fold increase (Figures 4B and 4C).

To further substantiate an H_2O_2-induced translation elongation block, wild-type and eIF2α^{S52A} mutant strains of *S. pombe* were subjected to brief glucose withdrawal to induce polysome run-off (Ashe et al., 2000; Figure S4C). After 1 h of exposure to H_2O_2, cells showed a decrease in polysomes that was more pronounced in wild-type cells relative to eIF2α^{S52A} mutant cells (Figure 4D). Glucose depletion of H_2O_2-treated wild-type cells led to complete polysome run-off (Figure 4D). In contrast, eIF2α^{S52A} cells maintained substantial polysome levels under the same conditions, indicating reduced translation elongation (Figure 4D). Taken together, these data strongly suggested that oxidative stress induces a block in translation elongation that is especially apparent in cells unable to phosphorylate eIF2α.

eEF2K Signaling Is Upregulated under H_2O_2-Induced Oxidative Stress in the Absence of eIF2α Phosphorylation

We next assessed the potential involvement of negative regulators of translation elongation, specifically the kinase that phosphorylates translation elongation factor eEF2 (eEF2K). Wild-type and eIF2α^{S51A} mutant MEFs were subjected to various ER and oxidative stress inducers followed by assessment of the inhibitory phosphorylation of eEF2 on threonine 56. eEF2 phosphorylation was induced in both wild-type and

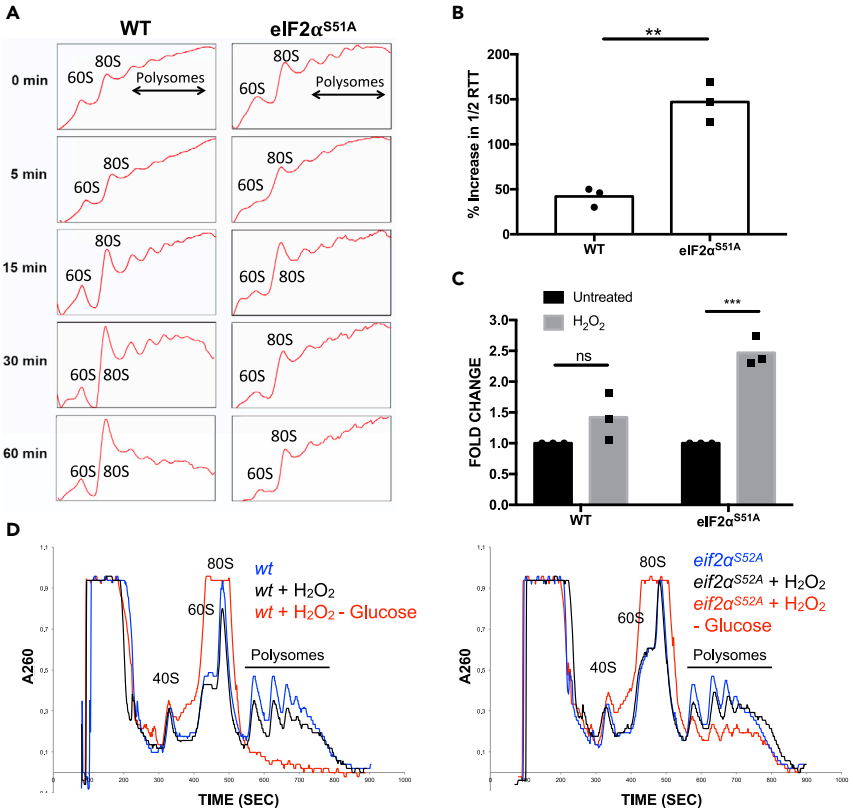

Figure 4. The Effects of Oxidative Stress on Translation Elongation

(A) Polysome profiling was done with wild-type and eIF2α^{S51A} mutant MEFs treated with 500 μM H_2O_2 for increasing periods (5–60 min).

(B) Ribosome transit times were analyzed in wild-type and eIF2α^{S51A} mutant MEFs treated with 500 μM H_2O_2. The graph represents the mean percent increase in 1/2 transit times ± standard deviations of at least three independent experiments each done in triplicates. *p value = 0.006. Statistical significance was determined by t test.

(C) The graph represents the normalized mean fold change of 1/2 transit times ± standard deviations of the same experiments as shown in Figure 3B. *p value WT = 0.127, p value eIF2α^{S51A} = 0.0005. Statistical significance was determined by t test.

(D) Polysome profiles of wild-type and eIF2α^{S52A} mutant *S. pombe*. Cells were either untreated or treated with 1 mM H_2O_2 for 1 h followed by removal of glucose for 5 min.

eIF2α^{S51A} mutant MEFs treated with H_2O_2, TBHP, and DTT (Figures 5A and 5D). However, eEF2 phosphorylation in response to oxidants, particularly H_2O_2, was considerably more pronounced in eIF2α^{S51A} mutant MEFs (Figures 5A and 5D).

Dose-response studies revealed marked differences in the sensitivity of eEF2 phosphorylation to H_2O_2. eEF2 phosphorylation in wild-type MEFs peaked between 2 and 4 mM H_2O_2 and coincided with eIF2α phosphorylation, whereas eEF2 phosphorylation was observed with as little as 0.5 mM H_2O_2 in eIF2α^{S51A} MEFs (Figures 5A and 5B). In both MEF lines, eEF2 phosphorylation subsided at high doses of H_2O_2, likely due to cytotoxicity (Figures 6B and 6C). No major cell line difference was observed in the sensitivity to H_2O_2-mediated changes in the phosphorylation of 4E-binding protein 1 (4E-BP1), which increased at low doses and subsided at high doses (Figures 5A and 5E). The finding that 4E-BP1 phosphorylation increased rather than decreased in response to H_2O_2 suggested that inhibition of TORC1 signaling is unlikely to be responsible for inhibiting translation under oxidative stress. The role of the paradoxical increase in 4E-BP1 phosphorylation in response to H_2O_2, which would be expected to promote eIF4E-eIF4G interaction and translation (Chu et al., 2016), remains presently unclear.

Time course experiments also revealed a marked difference in the kinetics of eEF2 phosphorylation. Although phosphorylation was induced within 5 min of H_2O_2 exposure in both MEF lines, the response

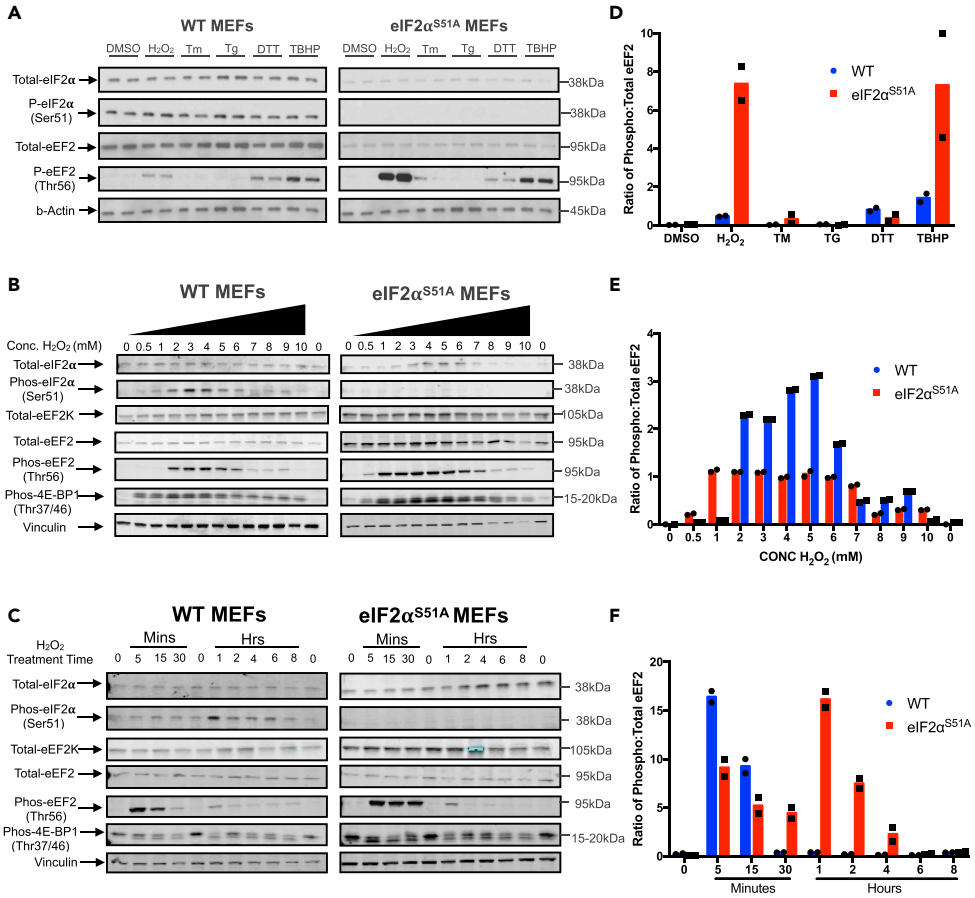

Figure 5. eEF2 Phosphorylation under Oxidative Stress

(A) Western blot analysis was performed with lysates from wild-type and eIF2α^{S51A} mutant MEFs. Cells were treated with the same agents as indicated in Figure 2C. Cells were treated for 1 h except in the case of tunicamycin (Tm), which was added for 4 h.

(B) Western blot analysis was performed with lysates from wild-type and eIF2α^{S51A} mutant MEFs treated with increasing doses of H_2O_2 (0.5–10 mM) for 1 h.

(C) Western blot analysis was performed with lysates from wild-type and eIF2α^{S51A} mutant MEFs treated with 500 μM H_2O_2 for increasing periods (5 min–8 h).

(D) Quantification of eEF2 phosphorylation. The graph represents the ratio of phosphorylated to total eEF2 quantified from the western blots in Figure 5A. The intensities were quantified using Licor Image Studio software. The individual symbols represent individual data points. The individual data points represent duplicated individual repeat experiments.

(E) Quantification of eEF2 phosphorylation. The graph represents the ratio of phosphorylated to total eEF2 quantified from the western blots in Figure 5B. The intensities were quantified using Licor Image Studio software. The individual symbols represent individual data points. The individual data points represent duplicated individual repeat experiments.

(F) Quantification of eEF2 phosphorylation. The graph represents the ratio of phosphorylated to total eEF2 quantified from the western blots in Figure 5C. The intensities were quantified using Licor Image Studio software. The individual symbols represent individual data points. The individual data points represent duplicated individual repeat experiments.

was more sustained in eIF2α^{S51A} MEFs (Figures 5C and 5F). H_2O_2-induced eIF2α phosphorylation in wild-type MEFs, which we determined to be mediated, at least to a large extent, by PERK (Figure S4), did not peak until 1 h after stress application, indicating that it may have a function in maintaining the translation block for increased periods. In summary, these data show that eEF2 phosphorylation occurs in an acute yet transient manner under oxidative stress. Conversely, eIF2α phosphorylation is delayed but more sustained.

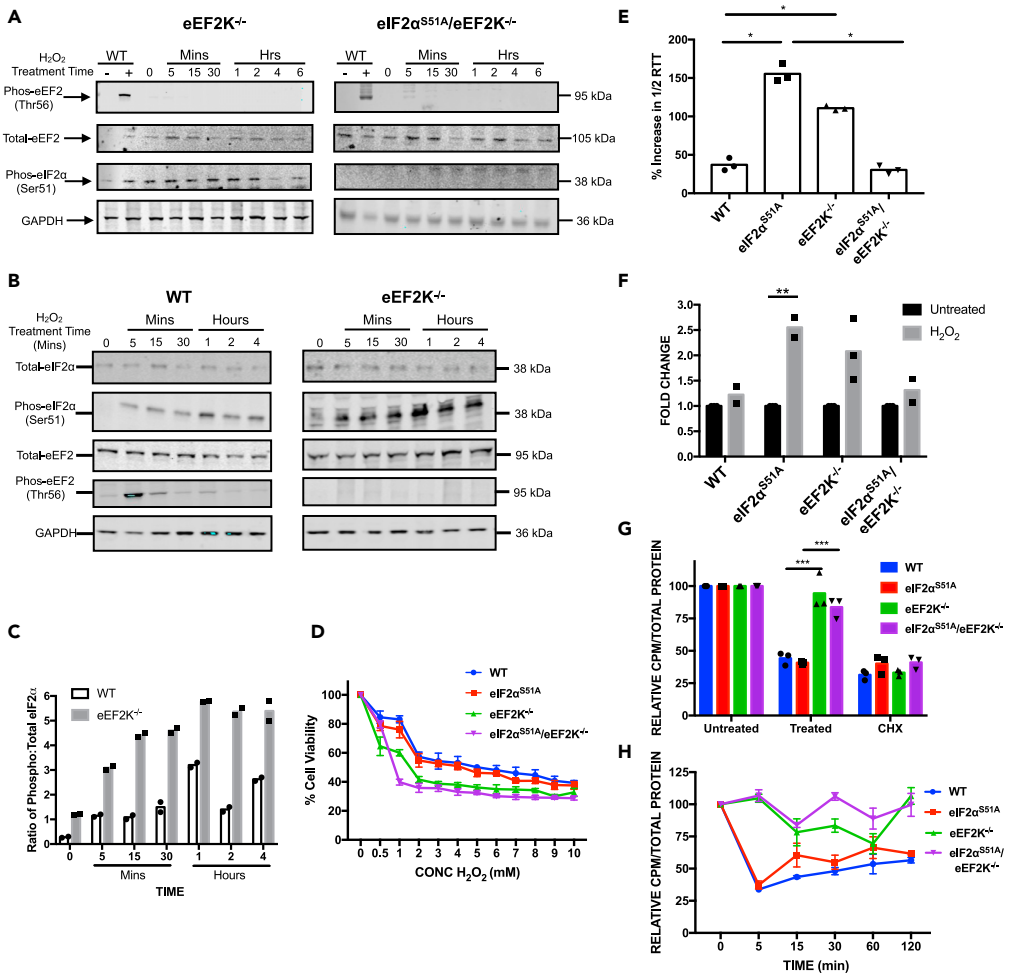

Figure 6. Role of eEF2K in eIF2α-Independent Translational Inhibition

(A) Western blot analysis was performed with lysate prepared from eEF2K$^{-/-}$ and eIF2α^{S51A}/eEF2K$^{-/-}$ MEFs treated with 500 μM H_2O_2 for increasing periods (5 min–6 h). Untreated WT MEFs were used as a negative control and WT MEFs treated with 500 μM H_2O_2 for 5 min were used as a positive control.

(B) Wild-type and eEF2K$^{-/-}$ MEFs were exposed to 500 μM H_2O_2 for increasing periods (5 min–4 h), and eIF2α phosphorylation was assessed by immunoblotting.

(C) Quantification of eIF2α phosphorylation. The graph represents the ratio of phosphorylated to total eIF2α quantified from the western blots in Figure 6B. The intensities were quantified using Licor Image Studio software. The individual symbols represent individual data points. The individual data points represent duplicated individual repeat experiments.

(D) Cells were treated with the indicated doses (0.5–10 mM) of H_2O_2 for 1 h. An MTT assay was performed to assess cell viability; see Figure S2C for verified results. The graph represents the means ± standard deviations of eight replicates.

(E) Ribosome transit times were analyzed in wild-type, eIF2α^{S51A}, eEF2K$^{-/-}$, and eIF2α^{S51A}/eEF2K$^{-/-}$ MEFs treated with 500 μM H_2O_2. The graph represents the mean percent increases in 1/2 transit times ± standard deviations of three independent experiments each done in technical triplicates. The individual symbols represent summaries of the individual experiments. *p value between WT and eIF2α^{S51A} = 0.017, p value between WT and eEF2K$^{-/-}$ = 0.044, p value between eIF2α^{S51A} and eEF2K$^{-/-}$ = 0.024. Statistical significance was determined by t test.

(F) The graph represents the normalized mean fold change of 1/2 transit times ± standard deviations of the same experiments as shown in Figure 6D. The individual symbols represent summaries of the individual experiments. *p value WT = 0.313, p value eIF2α^{S51A} = 0.007, p value eEF2K$^{-/-}$ = 0.108, p value eIF2α^{S51A}/eEF2K$^{-/-}$ = 0.314. Statistical significance was determined by t test.

(G) Cells were treated with 1 mM H_2O_2 or 50 μg/mL CHX or untreated. After 15 min, [^{35}S]-methionine was added for an additional 45 min. Protein synthesis levels were then quantified and adjusted according to the total amount of protein. The graph represents normalized means ± standard deviations of at least two independent experiments each done in

Figure 6. *Continued*

technical triplicates. The individual symbols represent summaries of the individual experiments. *p value eEF2K$^{-/-}$ = 0.004, p value eIF2α^{S51A}/eEF2K$^{-/-}$ = 0.0007. Statistical significance was determined by t test.

(H) Cells were treated with 1 mM H_2O_2 for increasing times indicated and labeled with [^{35}S]-methionine for 5 min. Protein synthesis levels were then quantified and adjusted according to the total amount of protein. The graph represents the normalized means ± standard deviations of at least two independent experiments each done in technical triplicates.

eEF2K Knockout Mouse Embryonic Fibroblasts Are Deficient in Attenuating Translation under Oxidative Stress

To establish a possible functional role of eEF2K in eIF2α-independent translation regulation under oxidative stress, eEF2K was knocked out using the CRISPR-Cas9 system in wild-type and eIF2α^{S51A} MEFs. When challenged with 500 μM H_2O_2 for 5 min to 6 h, neither cell line exhibited eEF2 phosphorylation (Figure 6A). Comparing wild-type and eEF2K$^{-/-}$ MEFs, we found that basal and H_2O_2-induced eIF2α phosphorylation is considerably augmented in cells lacking eEF2K (Figures 6B and 6C). Treatment of eEF2K$^{+/+}$ and eEF2K$^{-/-}$ MEFs with increasing concentrations of H_2O_2 (0.5–10 mM for 1 h) revealed increased sensitivity of both eEF2K knockout lines to H_2O_2-induced cytotoxicity relative to their parental lines, with the eIF2α^{S51A} eEF2K$^{-/-}$ MEFs being the most sensitive (Figure 6D). The ∼2.5-fold increase in ribosome transit time observed in eIF2α^{S51A} MEFs treated with H_2O_2 was reduced to ∼2-fold in eEF2K$^{-/-}$ and less than 1.5-fold in eEF2K$^{-/-}$/eIF2α^{S51A} MEFs (Figures 6E and 6F). Continuous metabolic labeling during a 1-h challenge with H_2O_2 revealed that eEF2K$^{-/-}$ MEFs are unable to attenuate protein synthesis to the same extent as the parental wild-type and eIF2α^{S51A} MEFs (Figure 6G). The same result was obtained in 5-min pulse labeling experiments across a 2-h time course of H_2O_2 challenge (Figure 6H). Taken together, these data show that eEF2K is required for initiating translational inhibition under oxidative stress.

eEF2K Is Necessary for Inhibiting Translation under Oxidative Stress in *S. pombe*

To investigate whether eEF2K-mediated mechanism of translation inhibition is evolutionarily conserved, the role of eEF2K in protein synthesis under stress was studied in *S. pombe*. The *cmk2* gene, encoding the putative *S. pombe* orthologue of eEF2K, was deleted in wild-type and eIF2α^{S52A} mutant strains. By quantitative phosphoproteomics, we identified a 2.12 (±0.3)-fold increase in the phosphorylation of a putative MAPK site, serine 436, of Cmk2p after 15 min of exposure to H_2O_2, indicating that Cmk2p phosphorylation is H_2O_2 inducible (Figure S6E). In addition, loss of *cmk2* confers sensitivity to H_2O_2 (Sánchez-Piris et al., 2002).

Acute exposure to H_2O_2 revealed hypersensitivity of *Δcmk2* and *eIF2α^{S52A} Δcmk2* strains (Figure 7A). Both the *WT* and *eIF2α^{S52A}* strains showed decreased levels of protein synthesis comparable with the cycloheximide control (Figure 7B). The *Δcmk2* and *eIF2α^{S52A} Δcmk2* strains, however, exhibited significantly higher levels of translation compared with the wild-type and eIF2α^{S52A} strains (Figure 7B). Protein synthesis was also measured by short pulse labeling with [^{35}S]-methionine at various times after H_2O_2 (5 min–2 h). After 5 min, *WT* and *eIF2α^{S52A}* strains showed a >50% reduction in protein synthesis, whereas *Δcmk2* and *eIF2α^{S52A} Δcmk2* strains showed only a ∼25% reduction (Figure 7C). The same differential effect was seen at the 2-h time point when *Δcmk2* and *eIF2α^{S52A} Δcmk2* cells had partially recovered protein synthesis. Unlike MEFs deficient in eEF2K, *S. pombe* cells lacking *cmk2* still downregulated protein synthesis between 15 and 60 min after H_2O_2 challenge (Figure 7C). It is thus possible that a partially redundant eEF2 kinase exists in fission yeast, perhaps the calmodulin-dependent kinase, Cmk1p. Regardless, in both *S. pombe* and mammalian cells, eEF2K facilitates acute inhibition of translation in response to oxidative stress.

DISCUSSION

Significance of Blocking Translation Elongation in Response to Oxidative Stress

The main observation of the present study is that, unlike with ER stress, acute translational shutdown in response to oxidative stress occurs independently of eIF2α phosphorylation despite robust eIF2α kinase pathway activation. Rather, we demonstrate in MEFs that oxidative stress triggers rapid activation of eEF2K and inhibitory phosphorylation of eEF2 thus effecting a block in elongation. Although most known mechanisms of translational control are exerted at the level of initiation, more recently, control at the elongation step has come into focus (Richter and Coller, 2015). For example, genome-wide ribosome profiling in budding yeast has revealed that oxidative stress blocks elongation, especially in the first 50 codons (Gerashchenko et al., 2012; Wu et al., 2019). A slowdown of elongation was also described in *E. coli* under hyperosmotic stress (Dai et al., 2018). Together with our observations in MEFs, these findings suggest that a block

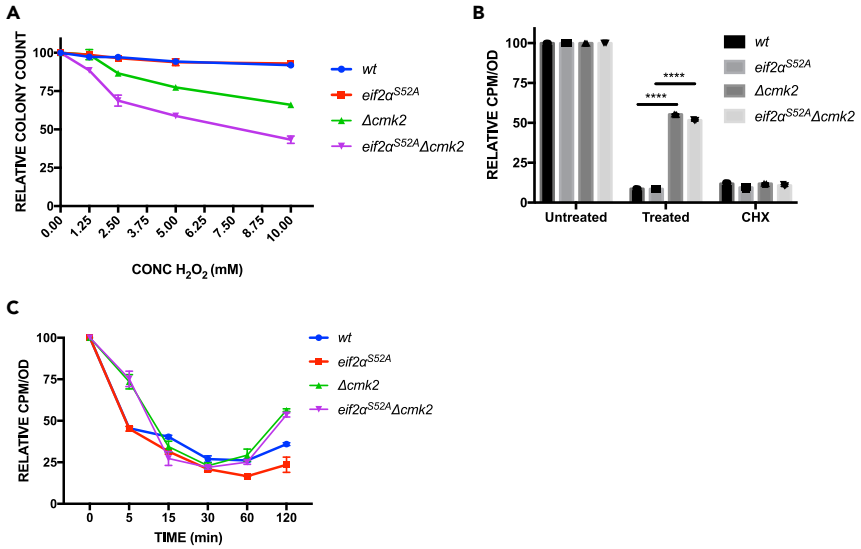

Figure 7. Effect of Hydrogen Peroxide on Viability and Protein Synthesis in *S. pombe cmk2* Mutants

(A) Cells were treated with increasing concentrations (0–1 mM) of H_2O_2 for 1 h. An equal number of cells were plated and grown for 3 days, and colonies were counted. The graph represents the mean ± standard deviations of at least two independent experiments each done in triplicates.

(B) Cells were treated with 1 mM H_2O_2 or 50 μg/mL CHX or untreated. After 15 min, [^{35}S]-methionine was added for an additional 45 min. Protein synthesis levels were quantified and adjusted according to the total amount of protein. The graph represents the normalized mean ± standard deviations of two independent experiments each done in triplicates. The individual symbols represent summaries of the individual experiments. *p value eEF2K$^{-/-}$ = 1.2 × 10^{-9}, p value eIF2α^{S51A}/eEF2K$^{-/-}$ = 9.4 × 10^{-9}. Statistical significance was determined by t test.

(C) Cells were treated with 1 mM H_2O_2 for the periods indicated and labeled with [^{35}S]-methionine for 5 min. Protein synthesis was quantified and normalized to the total amount of protein. The graph represents the normalized mean ± standard deviations of at least two independent experiments each done in triplicates.

in translation elongation is an evolutionarily conserved primary response to oxidative stress that may also be invoked under other stress conditions.

Temporally Distinct Roles of eIF2α and eEF2 Phosphorylation in MEFs

If eIF2α is dispensable for translational shutdown, does it have any role in the response to oxidative stress? Our genetic data indicate that yeast and mammalian cells deficient in both, eIF2α and eEF2 phosphorylation, are supersensitive to killing by H_2O_2 (Figures 6 and 7). It thus appears that both pathways cooperate in the defense against oxidative stress. Our kinetic data in MEFs show that eEF2 phosphorylation is a rapid and transient event (~5–15 min), whereas eIF2α phosphorylation peaks with a delay but is sustained (~1–6 h). This suggests a temporal ordering of both events with eEF2 triggering the initial block in protein synthesis and eIF2α phosphorylation maintaining it (Figure 8A). This conclusion is supported by our demonstration that cells deficient in eEF2 phosphorylation fail to initiate inhibition of protein synthesis, whereas MEFs deficient in eIF2α phosphorylation recover from the arrest precociously.

The reliance on the instant arrest in protein synthesis afforded by blocking elongation as compared with the delayed response achieved by a block in initiation suggests that the initial translational stress response is primarily geared toward limiting the accumulation of damaged nascent proteins, whereas the delayed response at the level of initiation may serve resource conservation purposes. Arresting ribosomes may also enable expedient resumption of elongation upon passing a putative quality control step thus being economically advantageous.

The timing difference in the eIF2α and eEF2 phosphorylation responses may be explained by distinct upstream triggers, a rapid kinase cascade in the case of eEF2K/eEF2, and the delayed accumulation of unfolded proteins in the case of PERK/eIF2α. The exact nature of the kinase cascade culminating in eEF2K activation remains unknown and may differ between stress conditions and organisms.

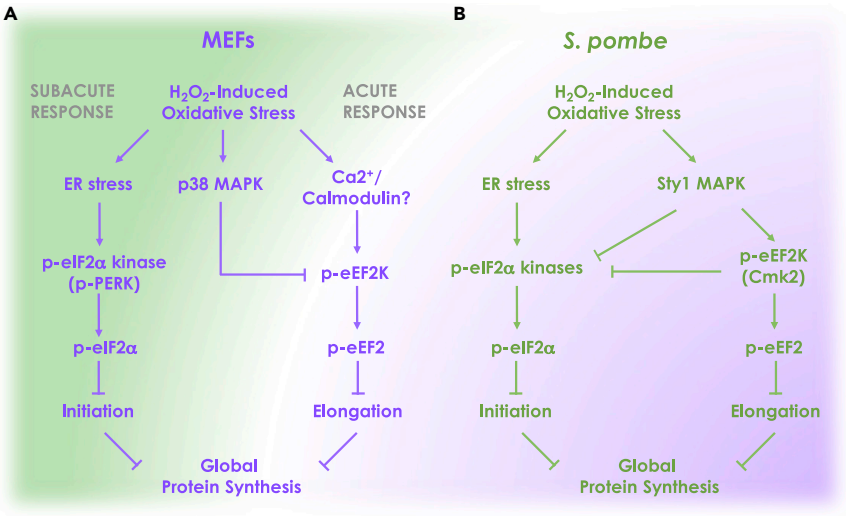

Figure 8. Model of the Conserved and Divergent Aspects of Stress-Induced Translation Inhibition Pathways in MEFs and *S. pombe*

(A) Model for MEFs. Oxidative stress triggers two parallel pathways. Rapid activation of eEF2K leads to acute arrest of translation elongation. The accumulation of misfolded proteins in the ER caused by oxidative stress triggers PERK-dependent eIF2α phosphorylation and subacute block in translation initiation. Signaling through p38 MAPK creates a negative feedback loop to terminate eEF2K signaling.

(B) Model for *S. pombe*. Oxidative stress rapidly induces both eIF2α phosphorylation and eEF2K activation. Sty1p MAPK activation triggers eEF2K signaling and creates a negative feedback loop to terminate eIF2α phosphorylation. There is also evidence that Cmk2p suppresses eIF2α phosphorylation.

Conserved versus Organism-Specific Response Patterns

Although eIF2α phosphorylation is dispensable for H_2O_2-induced translational shutdown in both MEFs and *S. pombe* due to a block in translation elongation, the responses also show marked organism-specific differences rendering the model in Figure 8A inapplicable to *S. pombe*. First, the kinetics of eIF2α phosphorylation are much faster in *S. pombe* than in MEFs with strong induction seen as early as 5 min after exposure to H_2O_2 (Berlanga et al., 2010; Dunand-Sauthier et al., 2005). Thus, phosphorylation of eIF2α and eEF2 appear to be initiated in parallel rather than in succession. Since H_2O_2-induced eIF2α phosphorylation lasts for at least 120 min (Krohn et al., 2008), it could theoretically play a role in maintaining the translation block. However, our data suggest that, in *S. pombe*, Cmk2p rather than eIF2α phosphorylation is required for maintenance of translational inhibition 2 h after H_2O_2 treatment (Figure 7C). This is consistent with data showing that Cmk2p attenuates eIF2α phosphorylation (Sanchez-Marinas et al., 2018).

A second marked difference between MEFs and *S. pombe* is in upstream signaling. The MAPK Sty1p is known to directly phosphorylate Cmk2p in response to H_2O_2 in *S. pombe* (Sánchez-Piris et al., 2002). At the same time, Sty1p activation limits eIF2α phosphorylation thus creating a negative feedback loop to terminate the translation arrest (Berlanga et al., 2010; Dunand-Sauthier et al., 2005) (Figure 8B). In contrast, although mammalian p38 MAPK kinase activity is also increased by H_2O_2 (Figure S5A), this kinase is known to inhibit rather than activate eEF2K (Knebel et al., 2002). Confirming this, we have found that MAPK inhibitors potently prolong H_2O_2-induced eEF2 phosphorylation in MEFs (Figure S5B). It thus appears that, unlike in *S. pombe*, oxidative stress activates eEF2K in an MAPK-independent fashion in mammalian cells. Since H_2O_2 increases intracellular calcium within seconds (Hu et al., 1998; Jornot et al., 1999), eEF2K may be directly activated by calmodulin in response to oxidative stress. Activation of p38 may subsequently act to terminate eEF2K activity for translation elongation to resume (Figure 8A).

Cross Talk between eIF2α and eEF2 Phosphorylation in MEFs

The pattern of eEF2 phosphorylation in MEFs is markedly disturbed by the absence of eIF2α phosphorylation, indicating cross talk between the two translation regulatory pathways. Not only is eEF2 phosphorylation triggered at lower doses of H_2O_2 (0.5 versus 2 mM), but the response is also substantially prolonged (2 h versus 30 min). Thus, the pathway blocking elongation is hypersensitized and hyperactivated in the

absence of the pathway inhibiting initiation. The hyperactivation of eEF2 phosphorylation suggests an eIF2α phosphorylation-dependent sensing mechanism that activates a negative feedback loop to inhibit eEF2, perhaps mediated by p38 kinase (Figure 8A). The hypersensitization of eEF2 phosphorylation in cells deficient in eIF2α phosphorylation might be explained by an increased load of ROS or reduced anti-oxidant capacity in eIF2α^{S51A} mutant MEFs as indicated by the stress profile apparent in the RNA sequencing (RNA-seq) data at baseline.

The pattern of eIF2α phosphorylation was also disturbed in cells lacking eEF2K, showing hyperactivation by H_2O_2 (Figures 6B and 6C). Likewise, in *S. pombe*, eIF2α phosphorylation in response to oxidative stress is prolonged in *cmk2* deleted cells (Sanchez-Marinas et al., 2018), suggesting that eIF2α phosphorylation is intensified. This could simply be due to increased accumulation of misfolded proteins in cells deficient in acute elongation arrest of protein synthesis, although more intricate cross talk scenarios are also conceivable.

Implications for Cancer

Within the tumor microenvironment, cancer cells are frequently exposed to oxidative stress that arises from oncogenic stimulation, metabolic defects, hypoxia, and nutrient depletion (Gorrini et al., 2013). The ability to respond to oxidative stress is thus central to the survival of cancer cells. The pro-survival function attributed to the frequent overexpression of eEF2K in cancer has been proposed to be due to improved stress adaptation (Fu et al., 2014). Nutrient depletion, for example, leads to AMPK-dependent activation of eEF2K and a block in elongation, whereas loss of eEF2K hampers the growth of tumors in mice under caloric restriction (Leprivier et al., 2013). High eEF2K expression correlates with decreased overall survival in medulloblastoma (Leprivier et al., 2013) and, as our own data mining shows, in renal cancer (Figure S7). The data presented here demonstrate that eEF2K activation is also a rapid consequence of exposure to oxidative stress. Considering that many clinically used cancer therapeutics act by exerting oxidative stress, the status of the eEF2K pathway as well as its cross talk with the eIF2α phosphorylation pathway may set a threshold that determines therapeutic response. Both pathways, possibly in combination, therefore appear attractive cancer drug targets, although effective eEF2K inhibitors remain to be developed (Liu and Proud, 2016).

Limitations of the Study

One limitation of the present study is the use of WT and eIF2α^{S51A} mutant MEFs after long-term adaptation to tissue culture. Although these two cell lines are supposed to vary in only one amino acid residue in eIF2α, our mRNA expression profiles show many differences that point to more substantial divergence of the two MEF lines. Acute, inducible knockout of the eIF2α^{S51A} phosphorylation site would thus be preferable, but no such system is currently available. We have mitigated this deficiency by performing additional experiments in *S. pombe* cells, which support our main conclusions that eIF2α phosphorylation is dispensable for translational arrest in response to H_2O_2, a response that is rather mediated by a block in translation elongation through eEF2K activation. A second limitation is that we observed higher-than-desirable variability in the response of eIF2α phosphorylation to H_2O_2. Although peak induction was consistently observed after ~1 h of H_2O_2 treatment, early time points showed greater variability. This might be due to slight but difficult-to-control variations in the stress status of individual MEF cultures as we sometimes observed considerable baseline activation of eIF2α phosphorylation in the absence of H_2O_2. Although this led to inconsistent quantifications at early time points, this limitation does not impact the main conclusions of our study. A final limitation is that we present tantalizing evidence of cross talk between eIF2α phosphorylation and eEF2 phosphorylation but the molecular mechanism mediating this cross talk remains to be determined in future studies.

METHODS

All methods can be found in the accompanying Transparent Methods supplemental file.

SUPPLEMENTAL INFORMATION

Supplemental Information can be found online at https://doi.org/10.1016/j.isci.2019.09.031.

ACKNOWLEDGMENTS

This research was funded by grants R21 CA190588, R01 GM105802, and R01 GM121834 (D.A.W.) and an F31 fellowship CA210616-01 (M.S.) from the U.S. National Institutes of Health (NIH). Part of this work was funded

by NIH P30 grants CA030199 and GM085764. D.A.W. is a scholar of the 1000 Talent Program funded by the Government of the People's Republic of China. We thank A.N.S. for her contribution. We thank Beata Grallert and Erik Boye for providing the *eIF2α*^{S52A} *S. pombe* strain, César de Haro for the *Δhri1 Δhri2 Δgcn2* strain, and Randal Kaufman for the eIF2α^{S51A} MEFs, syngeneic wild-type MEFs, and discussion.

AUTHOR CONTRIBUTIONS

Conceptualization, M.S. and D.A.W.; Methodology, M.S., A.R.C., C.-C.Y., P.A.B., and P.M.; Formal Analysis, M.S. and A.R.C.; Investigation, M.S., Y.L., C.-C.Y., A.R.C., P.M., and D.A.W.; Writing – Original Draft, M.S. and D.A.W.; Writing – Review & Editing, M.S., Y.L., C.-C.Y., A.R.C., P.M., and D.A.W.; Visualization, M.S.; Supervision, D.A.W. and P.A.B.; Funding Acquisition, M.S. and D.A.W.

DECLARATION OF INTERESTS

The authors declare no competing interests.

Received: February 15, 2019
Revised: June 14, 2019
Accepted: September 23, 2019
Published: October 25, 2019

REFERENCES

Ashe, M.P., De Long, S.K., and Sachs, A.B. (2000). Glucose depletion rapidly inhibits translation initiation in yeast. Mol. Biol. Cell *11*, 833–848.

Back, S.H., Scheuner, D., Han, J., Song, B., Ribick, M., Wang, J., Gildersleeve, R.D., Pennathur, S., and Kaufman, R.J. (2009). Translation attenuation through eIF2α phosphorylation prevents oxidative stress and maintains the differentiated state in beta cells. Cell Metab. *10*, 13–26.

Berlanga, J.J., Rivero, D., Martín, R., Herrero, S., Moreno, S., and de Haro, C. (2010). Role of mitogen-activated protein kinase Sty1 in regulation of eukaryotic initiation factor 2alpha kinases in response to environmental stress in *Schizosaccharomyces pombe*. Eukaryot. Cell *9*, 194–207.

Buttgereit, F., and Brand, M.D. (1995). A hierarchy of ATP-consuming processes in mammalian cells. Biochem. J. *312* (Pt 1), 163–167.

Carlberg, U., Nilsson, A., and Nygård, O. (1990). Functional properties of phosphorylated elongation factor 2. Eur. J. Biochem. *191*, 639–645.

Cheng, Y., Ren, X., Zhang, Y., Shan, Y., Huber-Keener, K.J., Zhang, L., Kimball, S.R., Harvey, H., Jefferson, L.S., and Yang, J.-M. (2013). Integrated regulation of autophagy and apoptosis by EEF2K controls cellular fate and modulates the efficacy of curcumin and velcade against tumor cells. Autophagy *9*, 208–219.

Chu, J., Cargnello, M., Topisirovic, I., and Pelletier, J. (2016). Translation initiation factors: reprogramming protein synthesis in cancer. Trends Cell Biol. *26*, 918–933.

Dai, X., Zhu, M., Warren, M., Balakrishnan, R., Okano, H., Williamson, J.R., Fredrick, K., and Hwa, T. (2018). Slowdown of translational elongation in *Escherichia coli* under hyperosmotic stress. MBio *9*.

Dunand-Sauthier, I., Walker, C.A., Narasimhan, J., Pearce, A.K., Wek, R.C., and Humphrey, T.C. (2005). Stress-activated protein kinase pathway functions to support protein synthesis and translational adaptation in response to environmental stress in fission yeast. Eukaryot. Cell *4*, 1785.

Fu, L.L., Xie, T., Zhang, S.Y., and Liu, B. (2014). Eukaryotic elongation factor-2 kinase (eEF2K): a potential therapeutic target in cancer. Apoptosis *19*, 1527–1531.

Gerashchenko, M.V., Lobanov, A.V., and Gladyshev, V.N. (2012). Genome-wide ribosome profiling reveals complex translational regulation in response to oxidative stress. Proc. Natl. Acad. Sci. U S A *109*, 17394–17399.

Gorrini, C., Harris, I.S., and Mak, T.W. (2013). Modulation of oxidative stress as an anticancer strategy. Nat. Rev. Drug Discov. *12*, 931–947.

Hershey, J.W.B., Sonenberg, N., and Mathews, M.B. (2012). Principles of translational control: an overview. Cold Spring Harb. Perspect. Biol. *4*.

Hiramatsu, N., Messah, C., Han, J., LaVail, M.M., Kaufman, R.J., and Lin, J.H. (2014). Translational and posttranslational regulation of XIAP by eIF2α and ATF4 promotes ER stress–induced cell death during the unfolded protein response. Mol. Biol. Cell *25*, 1411–1420.

Hu, Q., Corda, S., Zweier, J.L., Capogrossi, M.C., and Ziegelstein, R.C. (1998). Hydrogen peroxide induces intracellular calcium oscillations in human aortic endothelial cells. Circulation *97*, 268–275.

Jornot, L., Maechler, P., Wollheim, C.B., and Junod, A.F. (1999). Reactive oxygen metabolites increase mitochondrial calcium in endothelial cells: implication of the Ca2+/Na+ exchanger. J. Cell Sci. *112* (Pt 7), 1013–1022.

Kenney, J.W., Moore, C.E., Wang, X., and Proud, C.G. (2014). Eukaryotic elongation factor 2 kinase, an unusual enzyme with multiple roles. Adv. Biol. Regul. *55*, 15–27.

Knebel, A., Haydon, C.E., Morrice, N., and Cohen, P. (2002). Stress-induced regulation of eukaryotic elongation factor 2 kinase by SB 203580-sensitive and -insensitive pathways. Biochem. J. *367*, 525–532.

Knutsen, J.H.J., Rødland, G.E., Bøe, C.A., Håland, T.W., Sunnerhagen, P., Grallert, B., and Boye, E. (2015). Stress-induced inhibition of translation independently of eIF2α phosphorylation. J. Cell Sci. *128*, 4420–4427.

Krohn, M., Skjolberg, H.C., Soltani, H., Grallert, B., and Boye, E. (2008). The G1-S checkpoint in fission yeast is not a general DNA damage checkpoint. J. Cell Sci. *121*, 4047–4054.

Kruiswijk, F., Yuniati, L., Magliozzi, R., Low, T.Y., Lim, R., Bolder, R., Mohammed, S., Proud, C.G., Heck, A.J.R., Pagano, M., et al. (2012). Coupled activation-degradation of eEF2K regulates protein synthesis in response to genotoxic stress. Sci. Signal. *5*, ra40.

Lackner, D.H., Schmidt, M.W., Wu, S., Wolf, D.A., and Bähler, J. (2012). Regulation of transcriptome, translation, and proteome in response to environmental stress in fission yeast. Genome Biol. *13*, R25.

Lee, M.V., Topper, S.E., Hubler, S.L., Hose, J., Wenger, C.D., Coon, J.J., and Gasch, A.P. (2011). A dynamic model of proteome changes reveals new roles for transcript alteration in yeast. Mol. Syst. Biol. *7*, 514.

Leprivier, G., Remke, M., Rotblat, B., Dubuc, A., Mateo, A.-R.F., Kool, M., Agnihotri, S., El-Naggar, A., Yu, B., Somasekharan, S.P., et al. (2013). The eEF2 kinase confers resistance to nutrient deprivation by blocking translation elongation. Cell *153*, 1064–1079.

Liu, R., and Proud, C.G. (2016). Eukaryotic elongation factor 2 kinase as a drug target in cancer, and in cardiovascular and neurodegenerative diseases. Acta Pharmacol. Sin. *37*, 285–294.

Luo, J., Solimini, N.L., and Elledge, S.J. (2009). Principles of cancer therapy: oncogene and non-oncogene addiction. Cell *136*, 823–837.

McEwen, E., Kedersha, N., Song, B., Scheuner, D., Gilks, N., Han, A., Chen, J.-J., Anderson, P., and Kaufman, R.J. (2005). Heme-regulated inhibitor kinase-mediated phosphorylation of eukaryotic translation initiation factor 2 inhibits translation, induces stress granule formation, and mediates survival upon arsenite exposure. J. Biol. Chem. *280*, 16925–16933.

Nielsen, P.J., and McConkey, E.H. (1980). Evidence for control of protein synthesis in HeLa cells via the elongation rate. J. Cell. Physiol. *104*, 269–281.

Pavitt, G.D. (2018). Regulation of translation initiation factor eIF2B at the hub of the integrated stress response. Wiley Interdiscip. Rev. RNA *9*, e1491.

Richter, J.D., and Coller, J. (2015). Pausing on polyribosomes: make way for elongation in translational control. Cell *163*, 292–300.

Rolfe, D.F., and Brown, G.C. (1997). Cellular energy utilization and molecular origin of standard metabolic rate in mammals. Physiol. Rev. *77*, 731–758.

Sanchez-Marinas, M., Gimenez-Zaragoza, D., Martin-Ramos, E., Llanes, J., Cansado, J., Pujol, M.J., Bachs, O., and Aligue, R. (2018). Cmk2 kinase is essential for survival in arsenite by modulating translation together with RACK1 orthologue Cpc2 in *Schizosaccharomyces pombe*. Free Radic. Biol. Med. *129*, 116–126.

Sánchez-Piris, M., Posas, F., Alemany, V., Winge, I., Hidalgo, E., Bachs, O., and Aligue, R. (2002). The serine/threonine kinase Cmk2 is required for oxidative stress response in fission yeast. J. Biol. Chem. *277*, 17722–17727.

Sha, Z., Brill, L.M., Cabrera, R., Kleifeld, O., Scheliga, J.S., Glickman, M.H., Chang, E.C., and Wolf, D.A. (2009). The eIF3 interactome reveals the translasome, a supercomplex linking protein synthesis and degradation machineries. Mol. Cell *36*, 141–152.

Shenton, D., Smirnova, J.B., Selley, J.N., Carroll, K., Hubbard, S.J., Pavitt, G.D., Ashe, M.P., and Grant, C.M. (2006). Global translational responses to oxidative stress impact upon multiple levels of protein synthesis. J. Biol. Chem. *281*, 29011–29021.

Sonenberg, N., and Hinnebusch, A.G. (2009). Regulation of translation initiation in eukaryotes: mechanisms and biological targets. Cell *136*, 731–745.

Tavares, C.D.J., Ferguson, S.B., Giles, D.H., Wang, Q., Wellmann, R.M., O'Brien, J.P., Warthaka, M., Brodbelt, J.S., Ren, P., and Dalby, K.N. (2014). The molecular mechanism of eukaryotic elongation factor 2 kinase activation. J. Biol. Chem. *289*, 23901–23916.

Trachootham, D., Lu, W., Ogasawara, M.A., Nilsa, R.-D.V., and Huang, P. (2008). Redox regulation of cell survival. Antioxid. Redox. Signal. *10*, 1343–1374.

Trachootham, D., Alexandre, J., and Huang, P. (2009). Targeting cancer cells by ROS-mediated mechanisms: a radical therapeutic approach? Nat. Rev. Drug Discov. *8*, 579–591.

Tvegård, T., Soltani, H., Skjølberg, H.C., Krohn, M., Nilssen, E.A., Kearsey, S.E., Grallert, B., and Boye, E. (2007). A novel checkpoint mechanism regulating the G1/S transition. Genes Dev. *21*, 649–654.

Wek, R.C. (2018). Role of eIF2α kinases in translational control and adaptation to cellular stress. Cold Spring Harb. Perspect. Biol. *10*.

Wek, R.C., Jiang, H.-Y., and Anthony, T.G. (2006). Coping with stress: eIF2 kinases and translational control. Biochem. Soc. Trans. *34*, 7–11.

Wolf, D.A. (2014). Is reliance on mitochondrial respiration a "chink in the armor" of therapy-resistant cancer? Cancer Cell *26*, 788–795.

Wu, C.C.-C., Zinshteyn, B., Wehner, K.A., and Green, R. (2019). High-resolution ribosome profiling defines discrete ribosome elongation states and translational regulation during cellular stress. Mol. Cell *73*, 959–970.e5.

ISCI, Volume *20*

Supplemental Information

Cross Talk between eIF2α and eEF2 Phosphorylation Pathways Optimizes Translational Arrest in Response to Oxidative Stress

Marisa Sanchez, Yingying Lin, Chih-Cheng Yang, Philip McQuary, Alexandre Rosa Campos, Pedro Aza Blanc, and Dieter A. Wolf

SUPPLEMENTAL INFORMATION

SUPPLEMENTAL FIGURES AND LEGENDS

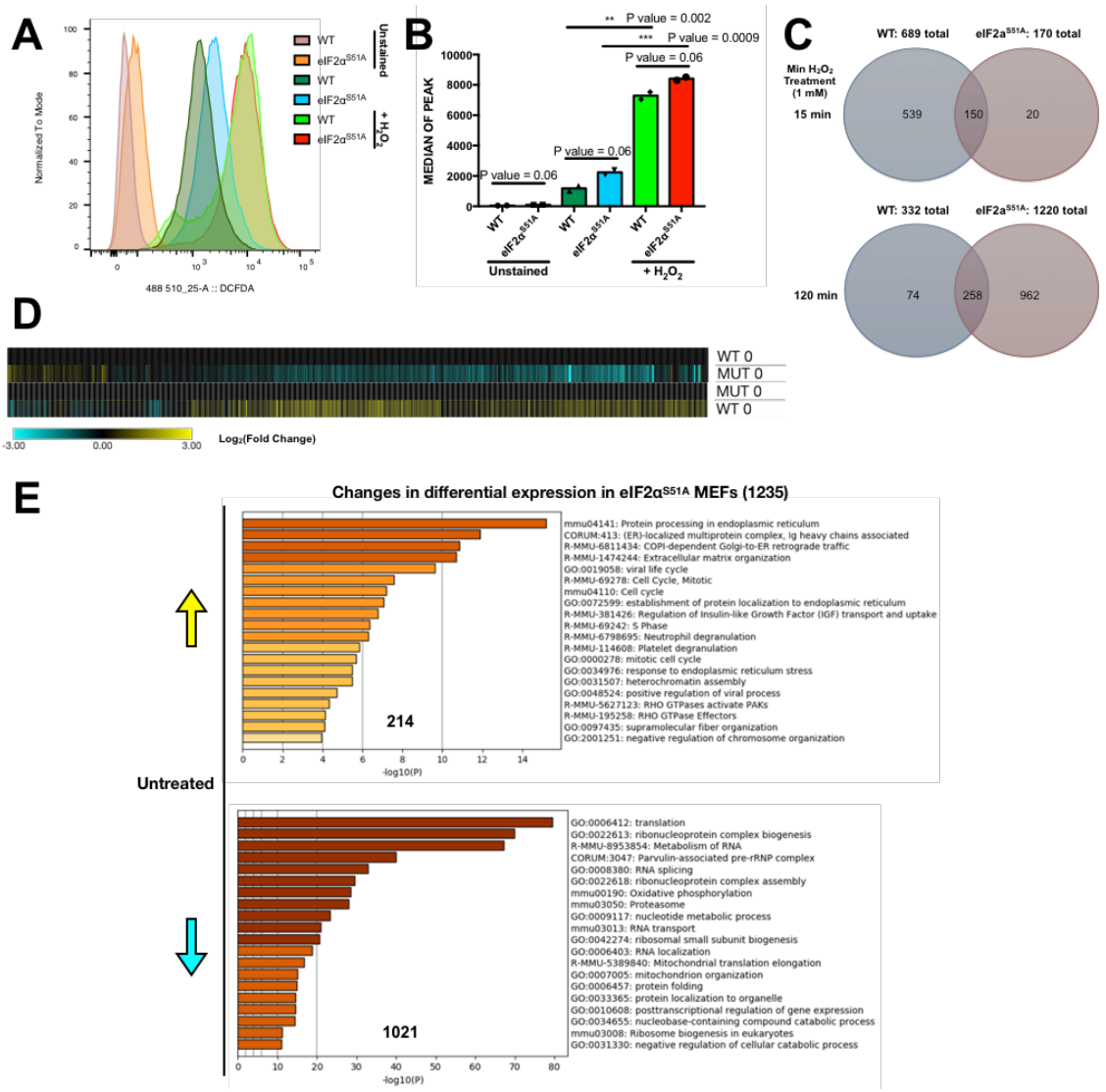

Figure S1. H_2O_2-induced changes in ROS and mRNA levels, Related to Figure 1.
(**A**) The effects of H_2O_2 on ROS levels. Cells were either untreated or treated with 500 μM H_2O_2 for 2 hrs. Cells were collected and stained with DCFDA for 30 minutes and FACS analysis was performed.
(**B**) The graph represents a duplicates, each individual symbol represents an individual data point. There is a fold change of 1.2 between the medians of WT and eIF2α^{S51A} MEFs treated with H_2O_2 and a fold change of 1.8 between the medians of untreated WT and eIF2α^{S51A} MEFs.
(**C**) Significant H_2O_2-induced changes in mRNA levels ($p \leq 0.05$) at both 15 and 120 minutes of H_2O_2 treatment (1 mM) were identified. There were 613 total changes occurring only in wildtype MEFs between both time points and 982 occurring only in eIF2α^{S51A} mutant MEFs at both time points. The total number of changes at each time point for each cell line include the overlap.
(**D**) Total RNA was extracted from WT and and analyzed by RNAseq. The data represents a compilation of significant changes in differential expression ($p \leq 0.05$) found in untreated WT and at baseline. Results are normalized to either untreated WT MEFs or untreated eIF2α^{S51A} MEFs at time 0 as indicated and displayed as a clustered heat map. Upregulated transcripts are shown in yellow and downregulated transcripts in blue.
(**E**) Individual lists of induced and repressed mRNAs (±3-fold change, $p \leq 0.05$) in eIF2α^{S51A} MEFs compared to WT MEFs were loaded into Metascape and the pathways enriched are indicated at time 0. Colored boxes represent either upregulated (yellow) or downregulated (blue) pathways.

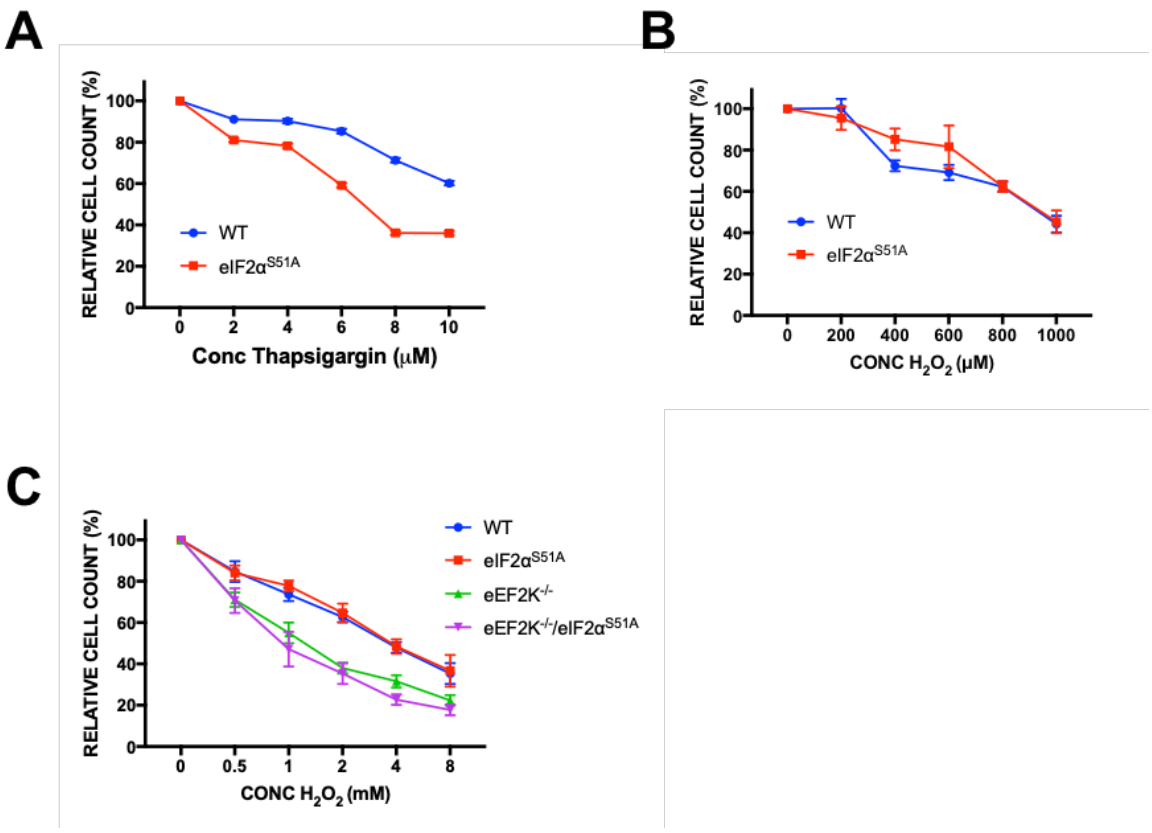

Figure S2. The effects of ER and oxidative stress on cell viability, Related to Figure 2 and Figure 6.

(**A**) MTT assay results in Figure 2A were validated by cell counting assay. The graph represents a summary of 3 individual experiments each performed in duplicates.

(**B**) MTT assay results in Figure 2B were validated by cell counting assay. The graph represents a summary of 3 individual experiments each performed in duplicates.

(**C**) MTT assay results in Figure 6D were validated by cell counting assay. The graph represents a summary of 3 individual experiments each performed in duplicates.

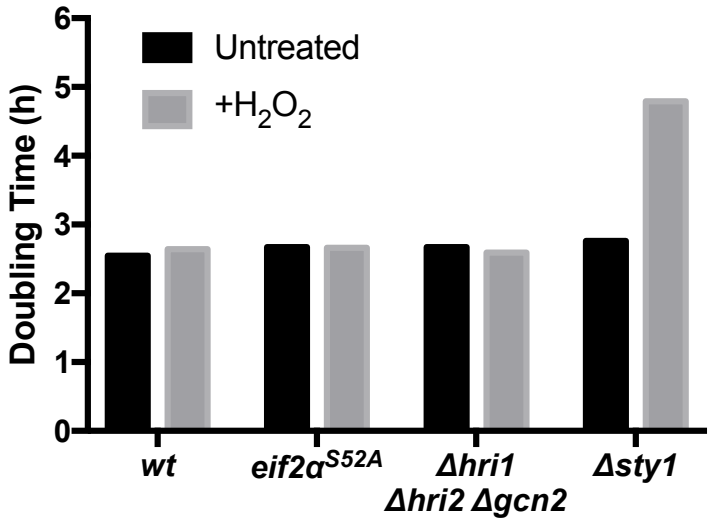

Figure S3. The effects of H_2O_2 on doubling time in *S. pombe*, Related to Figure 3.
S. pombe strains were treated with 1 mM H_2O_2 and grown for 24 hours. Doubling times were calculated based on OD measured at various time points.

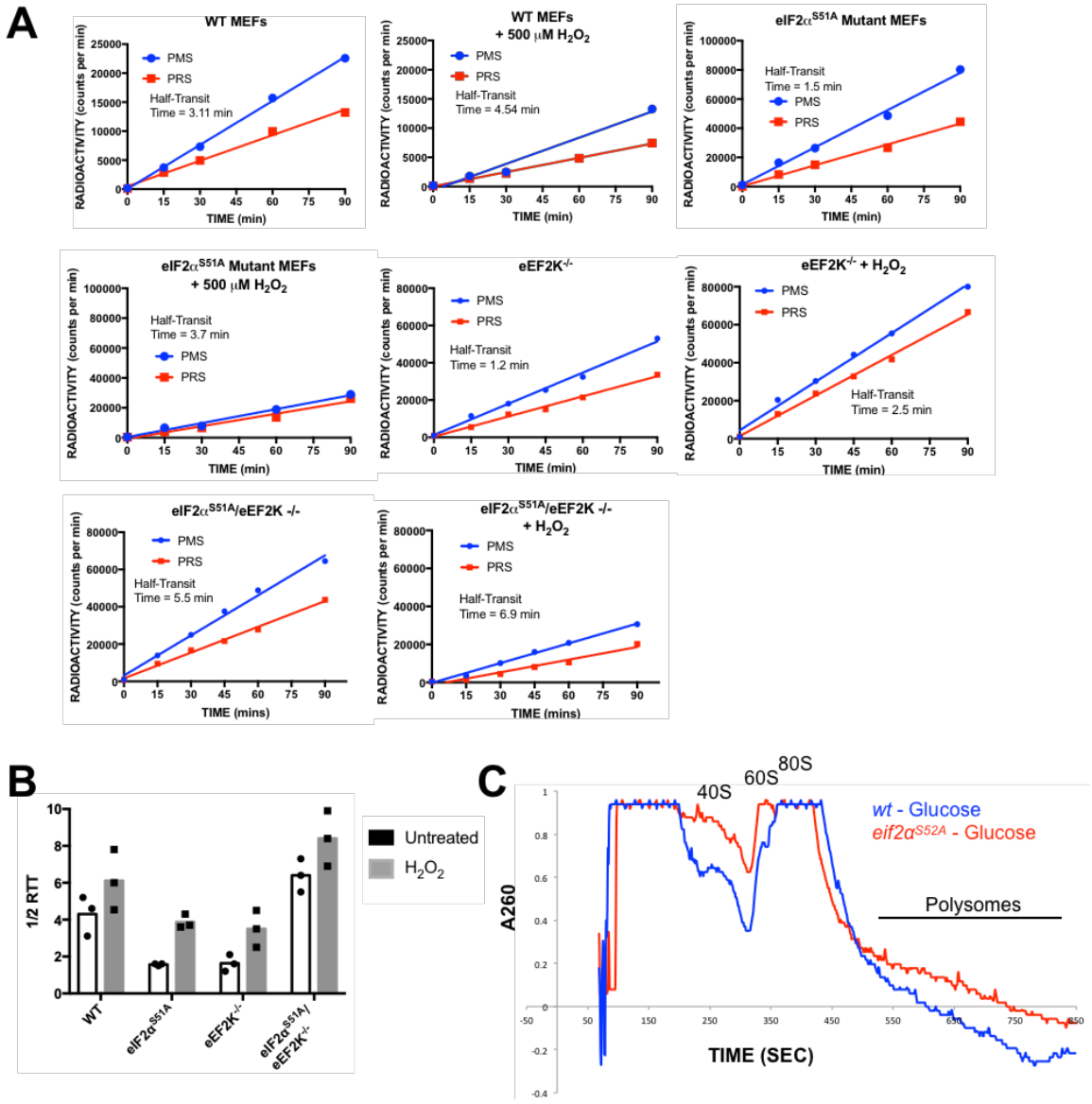

Figure S4. Additional elongation and initiation analysis, Related to Figure 4.
(**A**) Ribosome transit time experiments. The ribosome half-transit times of WT, eIF2α^{S51A}, eEF2K$^{-/-}$ and eIF2α^{S51A}/eEF2K$^{-/-}$ MEFs treated with and without 500 μM H_2O_2 were determined as described in Materials and Methods. Incorporation rates of [^{35}S]-methionine into total protein within the PMS and PRS was obtained by linear regression analysis, which was used to calculate half-transit times. Each experiment was performed three separate times.
(**B**) The graph represents a summary of each individual replicate experiment that was performed and the half-transit times (min) to obtain the results and statistical analysis represented in Figure 4B, 4C, 6C and 6D.
(**C**) Polysome profiles of *S. pombe* strains under glucose deprivation. *Wt* and *eIF2α*^{S52A} strains were deprived of glucose for 5 minutes and polysome profiles were acquired.

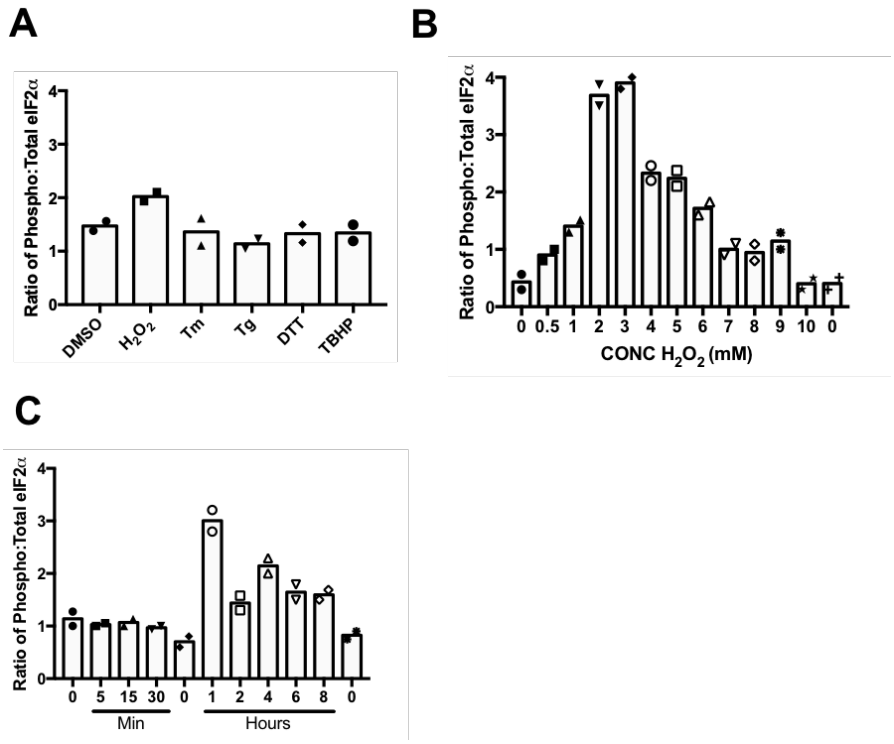

Figure S5. Quantification of eIF2α phosphorylation, Related to Figure 5.
(**A**) Quantification of eIF2α phosphorylation. The graph represents the ratio of phosphorylated to total eIF2α quantified from the Western blots representing WT MEFS in Figure 5A. The intensities were quantified using Licor Image Studio software. The individual symbols represent individual data points. The individual data points represent duplicated individual repeat experiments.
(**B**) Quantification of eIF2α phosphorylation. The graph represents the ratio of phosphorylated to total eIF2α quantified from the Western blots representing WT MEFS in Figure 5B. The intensities were quantified using Licor Image Studio software. The individual symbols represent individual data points. The individual data points represent duplicated individual repeat experiments.
(**C**) Quantification of eIF2α phosphorylation. The graph represents the ratio of phosphorylated to total eIF2α quantified from the Western blots representing WT MEFS in Figure 5C. The intensities were quantified using Licor Image Studio software. The individual symbols represent individual data points. The individual data points represent duplicated individual repeat experiments.

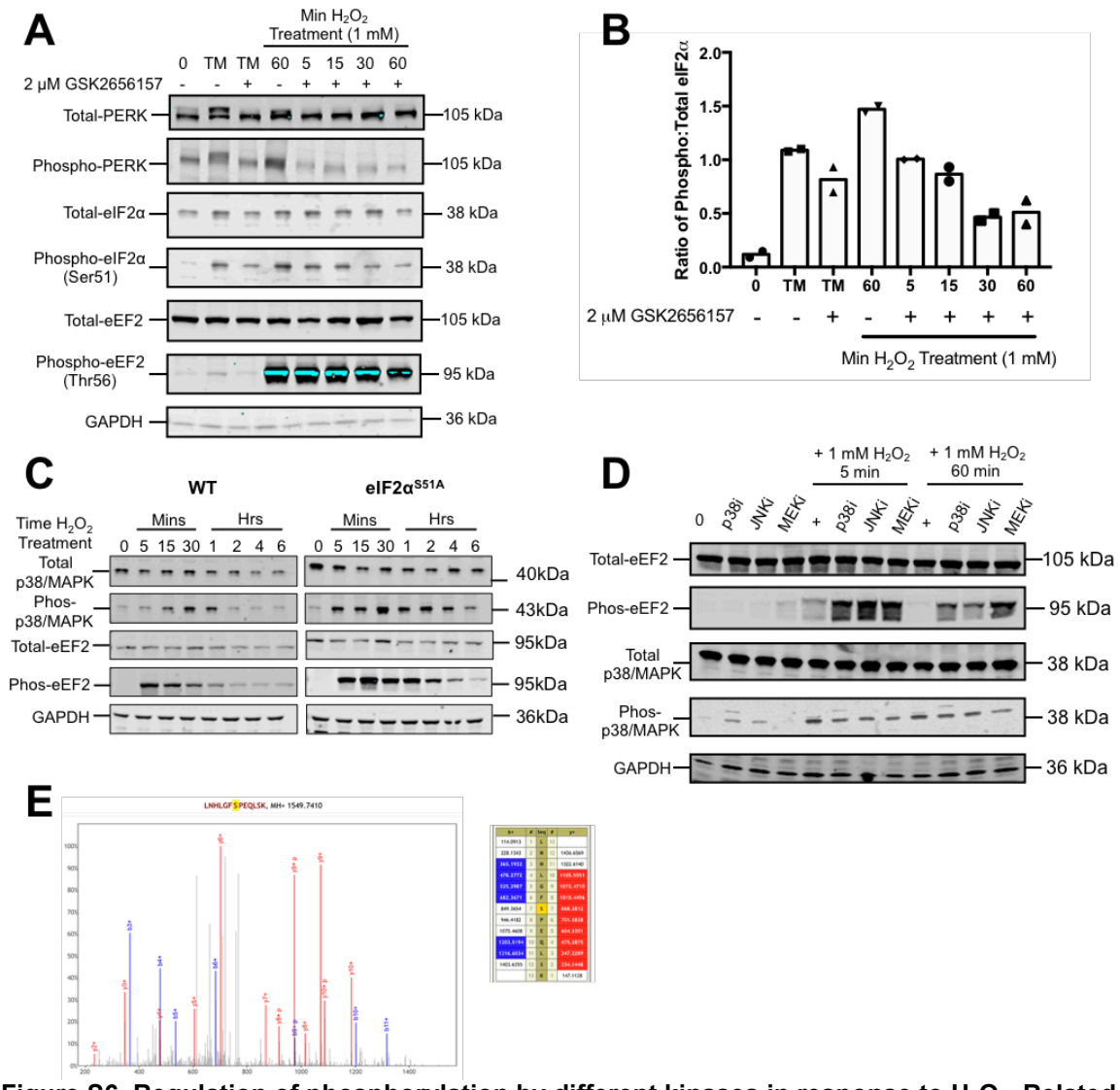

Figure S6. Regulation of phosphorylation by different kinases in response to H_2O_2, Related to Figure 7.

(**A**) Validation of PERK as the kinase that phosphorylates eIF2α under oxidative stress. WT MEFs were pre-treated for 1 hr with the PERK inhibitor GSK2656157 (2 μM) and as indicated and subsequently treated with 1 mM H_2O_2 for the indicated times. Western blot analysis was then performed.

(**B**) The graph represents quantification of Western blots from two separate experiments, including Figure S4A, using Licor imaging software. The individual symbols represent individual data points.

(**C**) The effects of p38/MAPK phosphorylation and inhibition on eEF2K under oxidative stress. Western blot analysis was done on WT and eIF2α^{S51A} MEFs treated with 1 mM H_2O_2 for the time points indicated.

(**D**) WT cells were pretreated with different MAPK inhibitors (p38i: SB203580, 20 μM, JNKi: SP600125, 40 μM, MEKi: U0126, 50 μM) for 1 hr followed by treatment with 1 mM H_2O_2 for the indicated times. Western blot analysis was performed.

(**E**) Mass spectrometric evidence for H_2O_2-triggered phosphorylation of serine 436 of *S. pombe* Cmk2p. Wildtype cells were exposed to H_2O_2 for 15 min, followed by preparation of cell lysate for phosphoproteomics (Singec et al., 2016). The mass spectrum shows evidence of phosphorylation of serine 436.

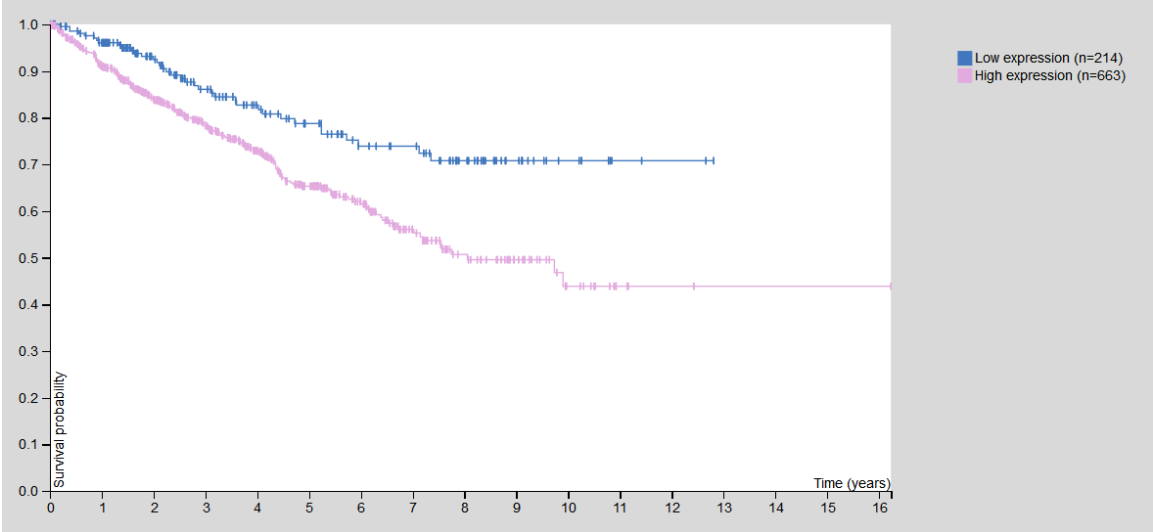

Figure S7. High levels of EEF2K mRNA correlate with decreased survival in renal cancer, Related to Figure 8.

Kaplan-Meier plots summarizing the results from analysis of correlation between mRNA expression level and patient survival. RNA-seq data is reported as median FPKM (number Fragments Per Kilobase of exon per Million reads), generated by The Cancer Genome Atlas (TCGA). Patients were divided based on level of expression into one of the two groups "low" (under cut off) or "high" (over cut off). FPKM cut off = 3.51. P = 0.00027. Data obtained through www.proteinatlas.com.

SUPPLEMENTAL TABLES

Table S1. *S. pombe* Strains, Related to Figure 3 and Figure 7.

Name	Genotype	Used in Fig.
WT	h+ ade6-M210 ura4-d18	3A, 3B, 3C, 3D, 4D, 6A, 7B, 7C, S3
eIF2α^{S52A}	h+ ade6-M210 eIF2alpha-S52A::ura4-d18	3A, 3B, 3C, 3D. 4D, 7A, 7B, 7C,
Δcmk2	h+ ade6-M210 ura4-d18 cmk2::NAT	7A, 7B, 7C,
eIF2α^{S52A} Δcmk2	h+ ade6-M210 eIF2alpha-S52A::ura4-D18 cmk2::NAT	7A, 7B, 7C,
Δhri1 Δhri2 Δgcn2	h- ade6- 216 leu1-32 ura4-d18 his7-366 hri1::ura4 hri2::leu1 gcn2::ura4	3A, 3B, 3C, 3D
Δsty1	h- leu1-32 ura4-d18 sty1::ura4	3C, 3D

Table S2. Reagents, Related to Figure 2, Figure 3, Figure 4, Figure 5, Figure 6 and Figure 7.

Reagent	Company	Cat. No.	Storage	Dilution/Conc
Hydrogen Peroxide	Sigma Aldrich	H1009-100mL	-20°C	0.1 – 1 mM
Tert-butyl hydroperoxide	Acros Organics	75-91-2	-20°C	200 µM
Cycloheximide	Acros Organics	66-81-9	-20°C	50 µg/mL
Tunicamycin	TOCRIS	351610	-20°C	10 µg/mL
Thapsigargin	TOCRIS	11381	-20°C	1 – 10 µM
DMSO	TOCRIS	3176	RT	
Dithiothreitol	Sigma Aldrich	3483-12-3	-20°C	10 mM
Anti-Total eIF2α	Cell Signaling	9722S	-20°C	1:1000
Anti- Phospho eIF2α (Ser51)	Cell Signaling	9721S	-20°C	1:500
Anti- Total eEF2	Cell Signaling	2332S	-20°C	1:1000
Anti- Phospho eEF2 (Thr56)	Cell Signaling	2331S	-20°C	1:500
Anti- GAPDH	GeneTex	GTX100118	-20°C	1:1000
Anti- b-Actin	GeneTex	GTX109639	-20°C	1:1000
Anti- Total eEF2K	Novus	NBP1-51329	-20°C	1:500
Anti- Phospho 4E-BP1 (Thr37/46)	Cell Signaling	2855P	-20°C	1:500
Anti- Vinculin	Sigma Aldrich	V4505-100UL	-20°C	1:1000
Anti- Total p38	Cell Signaling	9212	-20°C	1:1000
Anti- Phospho p38 (Thr180/Tyr182)	Cell Signaling	4631S	-20°C	1:500
Bovine Serum Albumin	Alpha Diagnostic Inc.	80400-100	-20°C	5%
Donkey anti Rabbit 680CW Secondary	LICOR	925-68073	-20°C, 4°C	1:10,000
Goat anti Mouse 680CW Secondary	LICOR	925-68070	-20°C, 4°C	1:10,000
Goat anti Rabbit 800CW Secondary	LICOR	925-32211	-20°C, 4°C	1:10,000
Goat anti Mouse 800CW Secondary	LICOR	925-32210	-20°C, 4°C	1:10,000

SUPPLEMENTAL DATA FILES

Metascape Analyses, Related to Figure 1.
RNAseq Analyses, Related to Figure 1.

TRANSPARENT METHODS

Reagents
Reagents are listed in Table S2.

Cell Lines and Tissue Culture
Wildtype and eIF2α^{S51A} Mutant Mouse Embryonic Fibroblasts (MEFs)
Both wildtype and eIF2α^{S51A} mutant mouse embryonic fibroblast cell lines were generously provided by Randal J. Kaufman. MEF cell lines were cultured in DMEM containing 4.5 mg/mL glucose (Invitrogen), 2.0 mM glutamine, 10% fetal bovine serum and 1% penicillin-streptomycin. Cells were incubated in 5% CO_2 at 37°C.

Generation of eEF2K Knockout and eEF2K$^{-/-}$/eIF2α^{S51A} MEFs
Wildtype and eIF2α^{S51A} mutant MEFs were transduced with a CRISPR/Cas9 lentiviral system containing pools of sgRNA libraries targeting the mouse eEF2K gene. Cells were transduced for 48 hours. Single cells were then sorted to generate monoclonal populations. Monoclonal cell lines were tested for functional eEF2K by Western blotting. To confirm eEF2K knockout, cellular DNA was isolated and genetic deletion was confirmed by PCR. Cell lines were also sequenced to further confirm eEF2K knockout in both wildtype and eIF2α^{S51A} mutant MEFs.

S. pombe Strains
Wildtype and eIF2α^{S52A} Mutant Strains
Strains were maintained in rich yeast extract medium with supplements (YES) or Edinburgh minimal media (EMM) at 30°C. Growth was measured using optical density at 596 nm. The genotypes of the strains used in this study are outlined in Table S1.

Generation of Δcmk2 and eIF2α^{S52A} Δcmk2 Strains
The deletion of *cmk2* was generated in wildtype and *eIF2α^{S52A}* mutant strains by PCR amplification of the plasmid pfa6a-NAT-HA. Cells were then transformed, selected on nourseothricin (NAT) plates, and *cmk2* knockout was confirmed by PCR.

MTT Cell Viability Assay
Cells were treated with indicated treatments or DMSO alone (0.1% final concentration) for indicated times. Viability was assessed by MTT assay (ATCC®) using the manufacturer's protocol. Briefly, 10 µl of MTT reagent was added to cells for 2 hrs. 100 µl of detergent reagent was then added to cells and the absorbance was read at 570 nm. Results are averages of 8 replicates ± standard deviations.

Protein Extraction and Western Blot Analysis
Mouse Embryonic Fibroblast Sample Preparation
For protein extraction, mammalian cells were washed once with 1x phosphate-buffered saline (PBS), scraped off and lysed in RIPA lysis buffer (50 mM Tris-HCl pH 8.0, 150 mM NaCl, 0.1% NP-40, 0.1% SDS and 12 mM sodium deoxycholate) supplemented with Halt™ Protease Inhibitor Cocktail (Thermo Scientific) and incubated on ice for 15 mins followed by sonication. After a 10 min centrifugation (13,000 rpm at 4°C), supernatants were taken for protein quantification following Pierce™ BCA Protein Assay Kit (Thermo Scientific). Samples were boiled with SDS sample buffer. Equal amounts of protein (20-40 µg) were resolved on 4-20% tris-glycine SDS–PAGE gels and transferred to nitrocellulose membranes, which were blocked in 5% bovine serum albumin (BSA) in 1x tris-buffered saline (TBS) (10 mM Tris-HCl pH 7.5, 150 mM NaCl) for 1 hr and then incubated with 5% BSA in TBST (10 mM Tris-HCl pH 7.5, 150 mM NaCl and 0.1% Tween 20) containing primary antibody overnight at 4°C. Membranes were washed (TBST 3×)

and incubated in TBST containing LICOR fluorescent secondary antibody. After washing (TBST 3×), immunoreactive bands were detected using the LICOR system.

S. pombe Sample Preparation
Yeast cells were cultured and collected in exponential growth phase (OD 0.5 – 1.0). Cells were centrifuged and resuspended in cold RIPA lysis buffer supplemented with Halt™ Protease Inhibitor Cocktail (Thermo Scientific) and added to 600 µl of zirconia/silica beads (BioSpec). Cells were ruptured in a FastPrep instrument for 40 sec at level 6. When necessary, supernatants were taken for protein quantification following Pierce™ BCA Protein Assay Kit (Thermo Scientific). Lysates were diluted with 2x SDS sample buffer and denatured at 95°C for 10 mins before loading. Western blot analysis was performed.

Protein Synthesis Fluorescence Assay
Protein synthesis levels were assessed in a non-radioactive manner by fluorescent protein synthesis assay (Protein Synthesis Assay Kit, Cayman Chemical) using the manufacturer's protocol. Briefly, corresponding treatments were added to cells for indicated times in a 96 well plate. Cycloheximide (50 µg/mL) was added for 1 hr as a positive control for protein synthesis inhibition. Cells were then incubated with O-propargyl-puromcyin (2.5 µg/mL) followed by fixation, washing (3x), and staining with 5 FAM-azide. Cells were then washed (3x) and fluorescence was detected with a fluorescent plate reader (excitation/emission = 485/535).

[^{35}S]-Methionine Labeling
Mouse Embryonic Fibroblast Sample Preparation
Cells were plated in 10 cm dishes at 3 × 10^6 cells/dish in supplemented DMEM, incubated overnight and treated with 500 µM H_2O_2 for indicated times. Cycloheximide (50 µg/mL) was added for 1 hr as a control for protein synthesis inhibition. Cells were then labeled with 10 µCi/mL [^{35}S]-methionine (EasyTag™ EXPRESS^{35}S Protein Labeling Mix, Perkin Elmer) for 5 mins, rinsed once with cold 1x PBS and harvested immediately by scraping. Cells were pelleted and resuspended in 0.5 mL lysis buffer (25 mM Tris-HCl pH 8.0, 150 mM NaCl, 0.1% NP-40, 0.1% SDS and 12 mM sodium deoxycholate) supplemented with Halt™ Protease Inhibitor Cocktail (Thermo Scientific). Lysates were boiled at 95°C for 10 mins, briefly centrifuged and blotted on Whatman filter paper for total protein precipitation. Filters were precipitated with ice-cold 20% TCA for 10 mins followed by 10% TCA for 5 mins. Filters were rinsed twice with 100% ethanol for 5 mins and air-dried. Radioactivity levels were determined by liquid scintillation counting. Total cellular protein was quantified with Pierce™ BCA Protein Assay Kit (Thermo Scientific) following the manufacturer's instruction. Incorporation of [^{35}S] methionine into total cellular protein was calculated and plotted.

S. pombe Sample Preparation
Yeast samples were centrifuged, resuspended in RIPA lysis buffer and added to 600 µl of zirconia/silica beads (BioSpec). Cells were ruptured in a FastPrep instrument for 40 sec at level 6. Lysates were diluted with 2x SDS sample buffer and denatured at 95°C for 10 mins before blotting.

Polysome Profile Analysis
Mouse Embryonic Fibroblast Sample Preparation
Cells (4 × 10^6) were seeded in 15 cm culture dishes and grown to ~70% confluence. Following treatment with 500 µM H_2O_2 at indicated time points, cycloheximide (CHX) (100 µg/mL) was added to cells for 5 min at 37°C. Cells were washed twice with cold 1x PBS containing CHX (100 µg/mL), scraped gently in 5 mL of ice cold 1x PBS containing CHX (100 µg/mL). Cells were centrifuged at 200 × g for 5 min at 4°C. The cell pellets were suspended in 0.45 mL of polysome lysis buffer (5 mM Tris-HCl at pH 7.5, 2.5 mM $MgCl_2$, 1.5 mM KCl). Lysis buffer was supplemented with 5 µl of 10 mg/mL CHX, 1 µl of 1 mM DTT, 100 units RNase inhibitor (RNaseOUT, Invitrogen), 1x Pierce™ protease inhibitor and 1x Pierce™ phosphatase inhibitor. Cells were vortexed for 5 sec followed by the addition of 25 µl 10% sodium deoxycholate and 25 µl Triton-X 100. Lysates were then vortexed again for 5 sec and centrifuged at 16,000 × g for 7

min at 4°C. Supernatants (cytosolic cell extracts) were collected and measured in absorbance of 260 nm. Approximately 10-15 ODs of lysates were layered over 5%–50% cold sucrose gradients in buffer (200 mM HEPES-KOH at pH 7.4, 50 mM MgCl2, 1 mM KCl, 100 µg/mL CHX and 1x Pierce™ protease inhibitor). Gradients were centrifuged at 39,000 rpm in a Beckman SW28 rotor for 2 hr at 4°C. After centrifugation, 14 equal-sized fractions (0.75 mL/fraction) were collected and analyzed through UV detection.

S. pombe Sample Preparation
Cells in exponential growth phase (OD 0.5 – 1.0) were treated with CHX (100 µg/mL) and centrifuged for 5 min at 2500 × g at 4°C. Cells were lysed in polysome lysis buffer (20 mM Tris-HCl [pH 7.5], 50 mM KCl, 10 mM $MgCl_2$, and 1 mM DTT) supplemented with 100 µg/mL CHX and 1x Pierce™ protease inhibitor. Lysates were added to 600 µl of zirconia/silica beads (BioSpec) and ruptured in a FastPrep instrument for 20 sec at level 6. Supernatants were extracted through centrifugation and polysome profiles were obtained.

Ribosome Half-Transit Time Measurement
Ribosome transit time refers to the length of time needed for a ribosome, after attaching to a mRNA, to complete translation and release a finished polypeptide. This is measured by analyzing the kinetic flow of radioactivity from polysome-bound (nascent) polypeptides to completed (released) polypeptides. Nascent and released polypeptides are separated by differential centrifugation. Since at any one time there is, on the average, one-half of a completed polypeptide per ribosome on a mRNA molecule, determination of the kinetics of flow of radioactivity as described will yield one half-transit time values. Measurements of half-transit times are completely independent of rates of attachment of ribosomes to mRNA and of the number of polyribosomes (Fan and Penman, 1970; Gehrke et al., 1981).

Cells (3×10^6) were plated in 10 cm dishes in supplemented DMEM and incubated overnight. Cells were simultaneously labeled with 10 µCi/mL [^{35}S]-methionine (EasyTag™ EXPRESS^{35}S Protein Labeling Mix, Perkin Elmer) and treated with 500 µM H_2O_2. At the times indicated, cells were washed with cold 1x PBS containing 100 µg/mL CHX and harvested immediately. Cells were pelleted and resuspended in 0.45 mL of lysis buffer (10 mM Tris-HCl at pH 7.5, 15 mM $MgCl_2$, 10 mM NaCl, 100 µg/mL CHX) supplemented with Halt™ Protease Inhibitor Cocktail (Thermo Scientific). Cells were lysed by adding 25 µl of 10% Triton X-100 and 25 µl 10% sodium deoxycholate, followed by vortexing for 5 seconds. Nuclei and mitochondria were pelleted by centrifugation for 15 min at maximum speed in a microfuge at 4°C. 200 µl of the post-mitochondrial supernatant (PMS) was saved to measure [^{35}S]-methionine incorporation into total protein (nascent and completed proteins). Ribosomes were pelleted by centrifugation of the remaining 200 µl of the PMS at 90,000 × g for 1 hr at 4°C in a Beckman TLA120 rotor. 200 µl of the post-ribosomal supernatant (PRS) were removed to measure the incorporation of [^{35}S]-methionine into completed protein. 50 µl of PMS and PRS samples from indicated time points were precipitated with TCA after spotting on Whatman filter paper. Filters were washed with ice-cold 20% TCA for 10 mins followed by 10% TCA for 5 mins. Filters were then rinsed twice with 100% ethanol for 5 mins and air-dried before being subjected to liquid scintillation counting.

RNA Sequencing
Total RNA from cells untreated or treated with 500 µM H_2O_2 at times 0, 15 minutes and 120 minutes was obtained using the RNeasy Mini Kit (Qiagen) following the manufacturer's instructions. RNA quality was assessed using a Bioanalyzer (Bio-Rad Experion), and RNA sequencing was performed at the Genomics Facility (Sanford Burnham Prebys Medical Discovery Institute) on the Illumina platform. The averaged expression data for ~10,000 mRNAs was narrowed down to ~1,600 mRNAs with significant differences in summed FPKM values of transcripts, p value ≤ 0.05. For each condition, these mRNAs were hierarchically clustered using Spearman Rank Correlation and Complete Linkage Clustering. A list of 613 mRNAs specific to WT MEFs that were significantly regulated (≥ 3-fold, p ≤ 0.05) by H_2O_2 was imported into Metascape (www.metascape.org) and canonical pathways enriched in the datasets were identified for all conditions in both cell lines (Figure 1B). A list of 982 mRNAs specific to eIF2α^{S51A} MEFs that were significantly regulated (≥ 3-fold, p value ≤ 0.05) by H_2O_2 was imported into

Metascape and canonical pathways enriched in the dataset were identified for all conditions in both cell lines (Figure 1C). The complete dataset is provided in Table S3 and available in the Gene Expression Omnibus (accession number GSE137409).

Statistical Analysis
Statistical analyses of replicate datasets were performed with Graphpad Prism. Typically, data were averaged, standard deviations calculated, and statistical significance was assessed using the T Test assuming two-tailed distribution and unequal variance.

Poly-A Fragment Sequencing
RNA sequencing was performed by the Genomics Core Facility at Sanford Burnham Prebys Medical Discovery Institute under the direction of Brian James. PolyA RNA was isolated using the NEBNext® Poly(A) mRNA Magnetic Isolation Module and barcoded libraries were made using the NEBNext® Ultra II™ Directional RNA Library Prep Kit for Illumina®(NEB, Ipswich MA). Libraries were pooled and single end sequenced (1X75) on the Illumina NextSeq 500 using the High output V2 kit (Illumina Inc., San Diego CA). Read data was processed in BaseSpace (basespace.illumina.com). Reads were aligned to to Mus musculus genome (mm10) using STAR aligner (https://code.google.com/p/rna-star/) with default settings. Differential transcript expression was determined using the Cufflinks Cuffdiff package (https://github.com/cole-trapnell-lab/cufflinks).

Metascape Pathway Enrichment Analyses (metascape.org)
User-provided gene identifiers are first converted into their corresponding M. musculus Entrez gene IDs using the latest version of the database (last updated on 2017-03-16). If multiple identifiers correspond to the same Entrez gene ID, they will be considered as a single Entrez gene ID in downstream analyses. For each given gene list, pathway and process enrichment analysis has been carried out with the following ontology sources: GO Biological Processes, KEGG Pathway, Reactome Gene Sets and CORUM. All genes in the genome have been used as the enrichment background. Terms with a p-value < 0.01, a minimum count of 3, and an enrichment factor > 1.5 (the enrichment factor is the ratio between the observed counts and the counts expected by chance) are collected and grouped into clusters based on their membership similarities. More specifically, p-values are calculated based on the accumulative hypergeometric distribution, and q-values are calculated using the Benjamini-Hochberg procedure to account for multiple hypotheses. Kappa scores are used as the similarity metric when performing hierachical clustering on the enriched terms, and sub-trees with a similarity of > 0.3 are considered a cluster. The most statistically significant term within a cluster is chosen to represent the cluster.

Western Blot Data Quantification
Licor imaging software was used to quantify Western blot band intensities. To quantify a given band, the total amount of signal detected in the area that contains the band is expressed as the sum of the intensities measured in all of these pixels. The signal value represents an unbiased estimate of specific signal intensity and is not affected by adjustments to the image display. A portion of this signal, however, corresponds to background, due to dark current, membrane reflection, autofluorescence, non-specific antibody binding, etc. Therefore, to estimate the amount of signal due only to the specific binding of the antibodies, a background subtraction is performed. To perform background subtraction, a background area surrounding the band is first defined. Within this area the average intensity of each pixel is calculated as an estimation of non-specific signal in the vicinity of the band of interest. This value is subtracted from the intensity of each pixel within the band area. The reported Signal value corresponds to the sum of the residual intensity values (after background subtraction) of all of the pixels in the band.

FACS Analysis
MEFs were either untreated or treated with 500 μM H_2O_2 for 2 hours. Cells were trypsinized and resuspended in media without FBS. Cells were treated with 20 μM 2',7'–dichlorofluorescin diacetate (DCFDA) for 30 minutes. Cells were then resuspended in cold 1 x PBS. FACS analysis

was performed by the Flow Cytometry Core at Sanford Burnham Prebys Medical Discovery Institute using the LSRFortessa.

Determination of doubling time of *S. pombe* cultures
S. pombe strains were inoculated into liquid YES media at an OD260 between 0.015 and 0.03 and grown for 24 hours. OD was measured at time 0, 5, 10, 21 and 23 hours and an exponential growth curve was fitted. The time to doubling the OD from 0.5 to 1 was calculated by solving the exponential equations for y -0.5 and y = 1.

Cell Counting Assay
Cells were treated with the indicated treatments for 1 hour, trypsinized and resuspended in media. Cells were diluted 1:2 in trypan blue and the number and concentration of viable cells was calculated using the Nexcelcom Bioscience Cellometer Auto T4 Bright Field Cell Counter and corresponding software.

Polysome Run-off by Glucose Withdrawal
In yeast, the action of glucose as a signaling molecule affects a diverse number of biochemical pathways. It has been shown that glucose depletion by means of glucose withdrawal from the growth medium led to a rapid, almost complete inhibition of protein synthesis. Re-addition of glucose causes a rapid reversal of this inhibition. The inhibition does not come about via a gross decay of mRNA, and neither the inhibition nor its reversal by re-addition of glucose requires transcription of new mRNAs (Ashe et al., 2000). The “runoff” of polysomes observed after glucose removal requires that translational elongation continues while initiation is inhibited (Mathews et al., 1996). Translational elongation of a polypeptide requires at least two GTP molecules per amino acid added, whereas initiation requires only one or two GTP molecules per polypeptide chain (Merrick and Hershey, 1996). It was also concluded glucose deprivation an effective way to block translation initiation independently of eIF2α phosphorylation (Ashe et al., 2000).

Cells in exponential growth phase (OD 0.5 – 1.0) were pelleted and resuspended in yeast extract medium without glucose and incubated at 30°C for 5 min. Cells were then with treated with CHX (100 µg/mL) and centrifuged for 5 min at 2500 × g at 4°C. Cells were lysed in polysome lysis buffer (20 mM Tris-HCl [pH 7.5], 50 mM KCl, 10 mM $MgCl_2$, and 1 mM DTT) supplemented with 100 µg/mL CHX and 1x Pierce™ protease inhibitor. Lysates were added to 600 µl of zirconia/silica beads (BioSpec) and ruptured in a FastPrep instrument for 20 sec at level 6. Supernatants were extracted through centrifugation and polysome profiles were obtained.

Data and Software Availability
RNA sequencing data: GEO: GSE137409

SUPPLEMENTAL REFERENCES

1. Ashe, M.P., De Long, S.K., Sachs, A.B., 2000. Glucose Depletion Rapidly Inhibits Translation Initiation in Yeast. Mol. Biol. Cell 11, 833–848.
2. Fan, H., Penman, S., 1970. Regulation of protein synthesis in mammalian cells. II. Inhibition of protein synthesis at the level of initiation during mitosis. J. Mol. Biol. 50, 655–670.
3. Gehrke, L., Bast, R.E., Ilan, J., 1981. An analysis of rates of polypeptide chain elongation in avian liver explants following in vivo estrogen treatment. I. Determination of average rates of polypeptide chain elongation. J. Biol. Chem. 256, 2514–2521.
4. Mathews M.B., Sonenberg N., Hershey J.W.B. 1996. Origins and targets of translational control. Translational Control. Cold Spring Harbor, NY: Cold Spring Harbor Laboratory; pp. 1–30.
5. Merrick W.C., Hershey J.W.B. 1996. The pathway and mechanism of eukaryotic protein synthesis. Translational Control. Cold Spring Harbor, NY: Cold Spring Harbor Laboratory; pp. 31–70.
6. Singec, I., Crain, A.M., Hou, J., Tobe, B.T.D., Talantova, M., Winquist, A.A., Doctor, K.S., Choy, J., Huang, X., La Monaca, E., Horn, D.M., Wolf, D.A., Lipton, S.A., Gutierrez, G.J.,

Brill, L.M., Snyder, E.Y., 2016. Quantitative Analysis of Human Pluripotency and Neural Specification by In-Depth (Phospho)Proteomic Profiling. Stem Cell Rep. 7, 527–542.